X-ray spectrometry of highly charged heavy ions in electron–ion rings

G. Zschornack, G. Musiol, M. Schiekel, and W. Wagner

Joint Institute for Nuclear Research, Dubna

Fiz. Elem. Chastits At. Yadra **21**, 1000–1042 (July–August 1990)

The electron–ion rings of the collective heavy-ion accelerator at the Joint Institute for Nuclear Research are considered as unique sources of highly charged ions. It is possible to obtain hydrogenlike ions of light and medium elements and, under optimal conditions, also ions of the heavy elements up to uranium. The emission of characteristic x rays is discussed. It is found that the use of the crystal-diffraction method is optimal for study of details of the atomic shells of highly charged ions. By spectrometry of the emitted characteristic x rays it is possible to satisfy the demand for information about such atoms by specialists in the fields of plasma physics and thermonuclear facilities, accelerators, laser technology, astrophysics, and a number of other applied fields.

INTRODUCTION

Ions of high degrees of ionization have become accessible to physical research comparatively recently. Progress in the creation of sufficiently powerful sources and the technical realization of new principles for obtaining highly ionized atoms have significantly extended the spectrum of available ions (compared with the possibilities provided by traditional ion sources), as regards both the atomic number Z and the degree of ionization I (Refs. 1–9). The new methods include deceleration of heavy ions accelerated and stripped by passage through thin foils (beam-foil method),[3] the cryogenic electron-beam method of ionization,[4,5] the method of highly ionized recoil ions,[6] laser-beam ionization,[7,8] and ionization in electron-cyclotron resonance.[9]

Thus, it has become possible to investigate a whole class of new physical phenomena, manifested, for example, in high-energy interactions of heavy ions with gas targets in ion–atom collisions[10,11] or in the neutralization on the surface of solids of slow ions almost completely stripped of their electrons.[12]

The volume of experimental data currently available on the structure of the electron shells and decay processes of hyperexcited multiply charged ions is as yet rather limited. This is explained by the technical difficulties of constructing the appropriate ion sources and the neccessary apparatus. To determine parameters such as the transition energies and the probabilities of decay through different channels, it is necessary to use delicate spectrometric methods with high resolution in order to separate the individual degrees of ionization of the ions or distinguish complicated electron configurations.

Therefore, our knowledge about the structure of highly charged ions has hitherto been based to a large degree on model calculations, made in the framework of a variety of approximations with allowance for the interactions of the shell electrons with the nucleus and with one another.[1] Experimental verification of the models is an extremely important and topical task in the deepening of our understanding of the interactions in "exotic" atomic states of this kind.[13]

The investigation of highly charged ions is also becoming increasingly important for practical purposes. Reliable atom–ion data are needed for the diagnostics of plasma facilities (for example, thermonuclear facilities) and the optimization of their construction and control,[14–21] for the investigation of ionization processes in ion sources,[4] for the effective use of heavy-ion accelerators,[11] for the interpretation of the spectra of astrophysical objects,[22] etc. Therefore, the increasing demand for atomic data is not surprising.

A qualitatively new source of highly charged ions is the ion-charged electron ring formed in the compression chamber of the collective heavy-ion accelerator developed at the JINR.[23] The relativistic electrons in the ring efficiently ionize atoms even in the inner, strongly bound electron states with large Z. If the dense electron ring is sustained for a sufficient time, it is possible to obtain ions of high ionization degree up to heliumlike ions of uranium.[24] Neutral atoms are injected into the compression chamber by means of a gas jet or sputtering by a laser ion source. Thus, the possibility is opened up of systematic investigations of the properties of highly charged ions in practically the entire periodic table.[25,26]

A specific feature of the ionization process in electron–ion rings is that with increasing time that the ring is maintained the mean degree of ionization of the ion ensemble increases, having at the same time a definite charge dispersion. Because of this the method of measurement must have a high resolution with respect to the degrees of ionization, and it is necessary to synchronize the measurement in time with the regime of the source; there must also be a definite degree of reproducibility of the parameters of the electron–ion rings. This makes it necessary to use remote spectrometry of the compression chamber in order to avoid an influence of the measuring instrument on the electron–ion ring and on the magnetic field that forms it.[28–30]

In view of these requirements, it is particularly promising to use the crystal-diffraction method of spectrometry of the characteristic x rays of the ions.[31] In this paper we discuss the measurement conditions for a focusing crystal-diffraction spectrometer (CDS) of Bragg type[32] for the compression chamber of the collective heavy-ion accelerator. It is concluded that several original experimental investigations of highly charged atoms can be made. The conclusions are important from the point of view of the diagnostics of the properties of the electron–ion rings of the accelerator, for

 0090-4759/90/040424-20$04.00

example, the determination of the number of ions in a ring, the charge dispersion, or the mean degree of ionization of the ion ensemble.

1. ELECTRON–ION RING AS A SOURCE OF HIGHLY CHARGED IONS

The principle of formation of the ion ring and its compression in the magnetic field of the compression chamber of the collective heavy-ion accelerator is described in detail in Ref. 23. If atoms or ions are injected into the ring, they are gradually stripped by collisional (direct and multiple) ionization by relativistic electrons and are captured by the electric space charge of the ring. The ionization cross sections of individual shells and the total ionization cross section were calculated as functions of the degree of ionization of the atom for ions of krypton, xenon, and uranium in Ref. 33. It was shown that, besides the direct ionization, processes such as the Auger and Coster–Kronig effects [80,81] can appreciably increase the rate at which the higher degrees of ionization are obtained, whereas the contributions from multiple direct ionization, as second-order ionization effects (double Auger effect, electron shake-off), decrease rapidly with decreasing degree of ionization.

The ionization cross sections calculated in Ref. 33 were used to calculate the time development of the degree of ionization of the ions in the electron–ion rings.[27] Figure 1 shows the ionization dynamics of xenon. The following conclusions were drawn in Ref. 27 about the use of the method of electron–ion rings as sources of highly ionized atoms. First, at each instant of time, measured from the time of injection of the atoms (or ions) into the compression chamber, ions of different charges exist simultaneously. In the case of heavy ions of moderate degree of ionization, the width of the charge distribution is on the average $\Delta I \approx$ 5–10 (Ref. 81), and if the observation time is restricted, then, because of the dynamics of the ionization process, the width of the charge distribution can be greater. Second, the characteristic time of ionization increases rapidly with increasing degree of ionization I. It is longer by 4–6 orders of magnitude for the inner shells ($I \approx Z$) than for weakly ionized atoms ($I \approx 1$).[33] As a result of this, the rate of decrease of the inization cross section is reduced for the highly charged ions. This means that the charge dispersion of the ion ensemble becomes narrower with increasing accumulation time of the ions, i.e., with increasing lifetime τ of the ring. However, to obtain high degrees I, in particular, for ions of heavy elements completely stripped of electrons, ring confinement times of the order of a second are needed, and this is technically difficult. In addition, there are restrictions from the point of view of the stability of the ring.[34]

However, calculations show that if there is additional compression of the ring, it is possible to obtain during a real ring confinement time $\tau \approx 50$ msec even the highest degrees I for the heavy elements: Xe^{54+}, U^{89+} (Refs. 34 and 35). It can also be seen from Fig. 1 how the intensity of a definite ion component varies in time. The "switching on" and "switching off" of definite charges of the ions are responsible for a restricted width of the charge distribution of the ions while there is a constant growth of the mean degree of ionization I. According to the calculations in Ref. 34, for an additional compression of the ring to $R = 1.5$ cm one can expect about 10^{11} Xe^{52+} ions or 5×10^{10} U^{84+} ions during a cycle of the compression chamber even for $\tau = 20$ msec if the ring contains $N_e \approx 10^{13}$ electrons and the small radii of the ring are $a = 0.1$ cm.

The yield of ions of a definite species is related to the ring neutralization factor:

$$f = N_i I / N_e, \tag{1}$$

where N_i is the number of ions in the ring. If a stable ring is maintained, I increases with the time (Fig. 1), and the condition of stability of the ring with respect to dipole oscillations imposes the restriction $f < 0.8$. Therefore, the yield of the higher degrees of ionization of the heavy ions must be lower than the yield of highly charged ions of lighter elements. If we plot I for all elements Z and keep as parameters the ring lifetime τ and the ring radius R, then we obtain below the curves in Fig. 2 the ionization states that are accessible. The uniqueness of the method of electron–ion rings as sources of ions of any element in a very wide range of degrees of ionization I is manifested particularly clearly when a sufficiently large ionization factor is realized. In Fig. 3 we compare the method of ionization in electron–ion rings with other modern methods for obtaining highly charged heavy ions with allowance for a sufficient level of ionization $n_e\tau$, where n_e is the electron density. Figure 4 shows for the example of xenon ions what fluxes can be expected.

2. ELECTRON–ION RING AS A SOURCE OF CHARACTERISTIC X RAYS OF IONS

Excitation and ionization of ions

The total cross section for ionization of ions by electrons is the sum of the partial cross sections for the production of holes in all subshells:

$$\sigma_{\text{tot}} = \sum_{nlj}{}' \sigma_{nlj}(Z, I), \tag{2}$$

where the contribution from the inner, more strongly bound electrons is smaller by several orders of magnitude than the

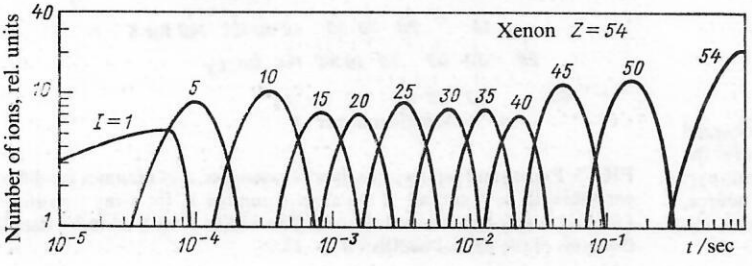

FIG. 1. Development of the degree of ionization of xenon ions in electron–ion rings.[27] The number of electrons is 1×10^{13}, the ring cross section is 0.12 cm^2, and the large radius of the ring is 4 cm; t is the time of confinement of the ring and accumulation of the ions and I is the degree of ionization.

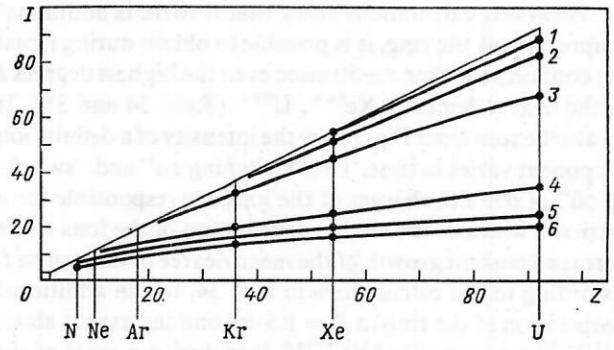

FIG. 2. Attainment of degree of ionization I for elements with atomic number Z as a function of the ring confinement time: 1) $\tau = 60$ msec, ring radius $R = 1.5$ cm; 2) $\tau = 30$ msec, $R = 1.3$ cm; 3) $\tau = 7$ msec, $R = 2.0$ cm; 4) $\tau = 3.5$ msec, $R = 4.0$ cm; 5) $\tau = 1$ msec, $R = 3.5$ cm; 6) $\tau = 4$ cm.

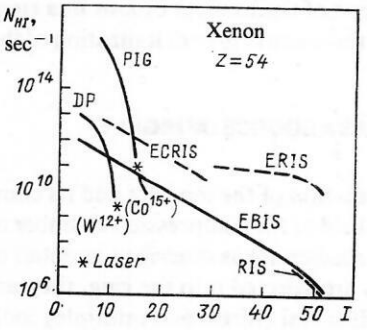

FIG. 4. Maximally achieved fluxes N_{HI} of ions in different sources with a high degree of ionization for the example of xenon: RIS, source of highly ionized recoil ions. For additional explanations, see Fig. 3 (based on Refs. 7 and 24).

contribution from the outer electrons.[33] If an electron is knocked out of an inner shell, the ion can shed its excitation by emitting characteristic x rays or Auger electrons. Let us estimate the states from which the ions radiate x rays and with what intensity. The number of excited ions N^* per unit time is determined by the formula

$$\frac{dN^*}{dt} = \sigma_E \frac{N_e}{2\pi^2 a^2 R} v_e, \qquad (3)$$

where a is the radius of the transverse section of the ring, R is the large radius of the ring, v_e is the electron velocity ($v_e \approx c$), and σ_E is the cross section for excitation of the ion. For $\sigma_E \approx 10^{-16}$ cm^2, a value that is certainly greater than the partial cross sections for ionization of all the subshells, accumulation time $\tau = 60$ msec, and ring parameters $a = 1$ mm, $R = 1.5$ cm (Ref. 34), the mean time between two excitation events is of order 10^{-16} sec. Since the characteristic times for filling of vacancies in the K, L, and M shells for $Z \geqslant 10$ are in the range $10^{-18} < t < 10^{-13}$ sec (Fig. 5), it can be assumed that the emission of the characteristic x rays takes place from the ground state of the ion. This means that in the electron–ion rings satellite x-ray lines of ions with outer vacancies arise.

Energy shifts of characteristic x rays

In an atom that has lost its outer electrons the binding energies of the remaining electrons are changed because of the partial lifting of the screening of the Coulomb potential of the nucleus and the interaction between the electrons. This effect is most strongly manifested in the inner orbitals responsible for the x-ray transitions. Systematic relativistic calculations of the electron binding energies were made by the self-consistent field method in the approximation of frozen orbitals with a local exchange potential of the electrons (Dirac–Fock–Slater method) for free ions of all elements Z and degrees of ionization I.[36] As a consequence of the change

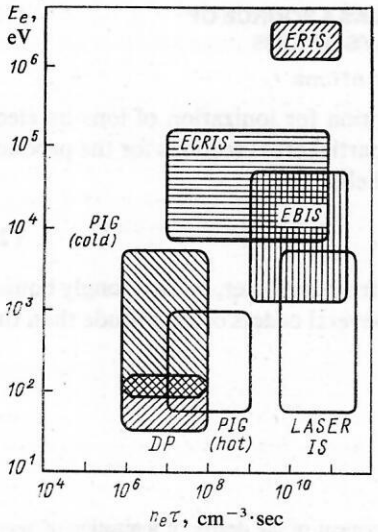

FIG. 3. Comparison of electron–ion rings as sources of highly charged ions (ERIS) with other modern heavy-ion sources, with allowance for the energy E_e of the ionizing electrons and the achieved ionization factor $n_e\tau$: PIG, Penning ion source; DP, duoplazmotron; LASER, laser source; EBIS, electron-beam source; ECRIS, electron-cyclotron resonance ion source.

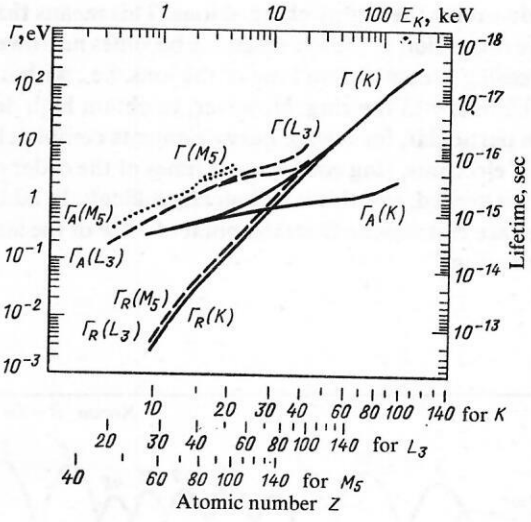

FIG. 5. Partial and total widths, binding energies, and lifetimes for different subshells as functions of the atomic number Z for x-ray transitions (R) and Auger-type transitions (A). The widths Γ with no index denote the sums of the partial widths ($R + A$).

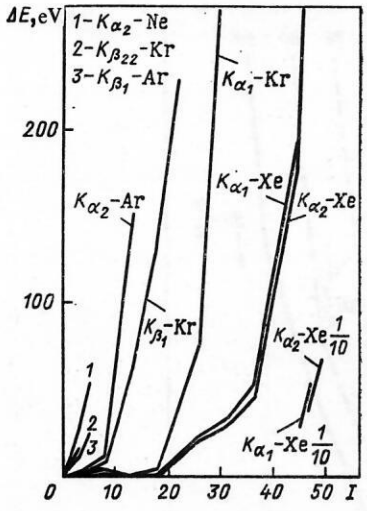

FIG. 6. Energy shifts ΔE of K transitions of characteristic x rays of noble gases as functions of the degree of ionization I.[37]

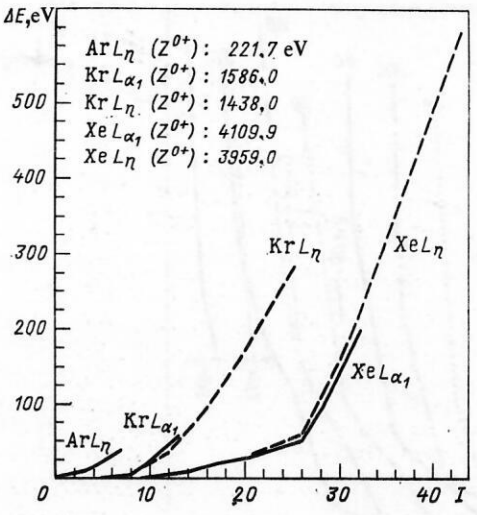

FIG. 8. Energy shifts ΔE of L transitions of the characteristic x rays of noble gases as functions of the degree of ionization I.[37]

of the binding energies, we observe corresponding energy shifts of the x-ray lines of the ions relative to the diagram lines of the neutral atoms.

As an example, Fig. 6 gives the shifts ΔE of some K lines of the noble gases Ar, Kr, and Xe as a function of the number of outer vacancies. For high degrees of ionization, the shifts of the x-ray lines reach 10^1–10^2 eV; the relative shift $\Delta E/E$ is 2–3% (Fig. 7), and it decreases with increasing Z because of the enhanced screening of the outer electrons. The same situation is shown in Figs. 8 and 9 for the lines of the L series. For the low degrees of ionization, the numerical values of the shifts of the lines are comparable with their natural widths, and it is not possible to resolve the neighboring satellites.

The absolute values of the energy shifts of the K_β and L lines for equal numbers of outer vacancies is greater than for the K_α lines (see Figs. 6 and 8). This is also observed for the relative shifts (see Figs. 7 and 9). At the same time, the transitions themselves have energy positions both below and above the K_α lines. As a rule, the appearance of outer vacancies has a stronger influence on the inner electrons. The partial lifting of the outer screening of the central field of the nucleus leads to a gain in the binding energy, particularly of the inner electrons. The nonmonotonic behavior of the shifts is due to ionization of the outer d or f electrons with extremely elongated orbits and low probability for their being near the nucleus.[38,39] The situation is demonstrated in Figs. 10 and 11 for the K_{α_1} and L_{α_1} lines of selected elements.

Broadening of characteristic x-ray lines by external fields

Figure 5 shows the behavior of the partial and total widths of the electron K, L, and M states as functions of the atomic number Z. The natural width of an x-ray line is made up of the partial radiative widths of the initial and final levels. Additional broading of the observed lines can be due to interaction of the electrons with external electric and magnetic fields. Indeed, the electron ring confines the ions by its own electric field. In addition, the ring itself is formed in the external magnetic field of the compression chamber ($\approx$2 T).

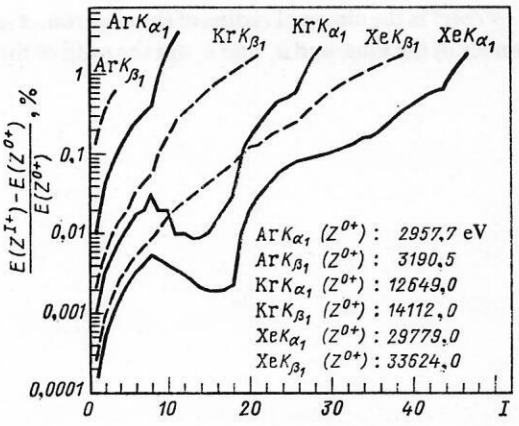

FIG. 7. Relative energy shifts of K_{α_1} and K_{β_1} lines for ions with degree of ionization I, compared with energies $E(Z^{0+})$ of the diagram lines.

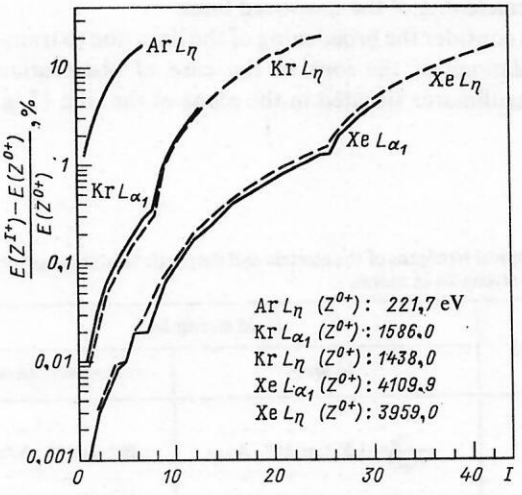

FIG. 9. Relative energy shifts of L_{α_1} and L_η lines of ions with degree of ionization I, compared with the energies $E(Z^{0+})$ of the diagram lines.

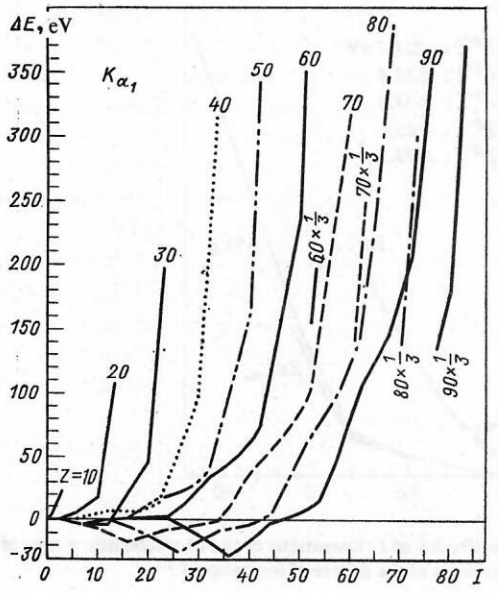

FIG. 10. Energy shifts ΔE for K_{α_1} transitions of some elements as functions of the degree of ionization I of the ion ground state.

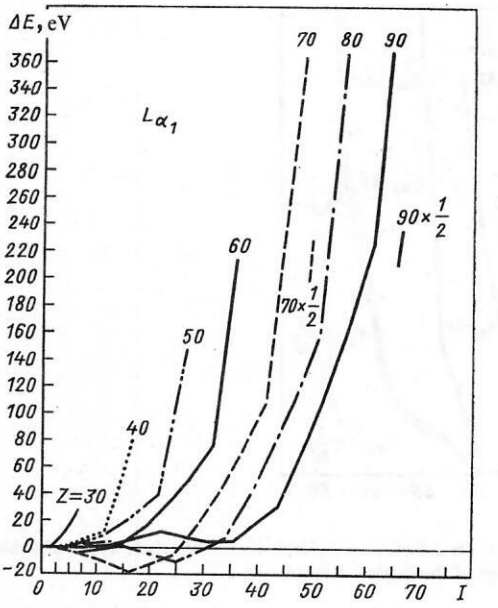

FIG. 11. Energy shifts ΔE for L_{α_1} transitions of some elements as functions of the degree of ionization I of the ion ground state.

Table I gives the typical strengths of the electric and magnetic fields that act on the ions as compared with the strengths of the self-fields in the atoms.

The splitting of the ion levels due to the Zeeman and Stark effects at these strengths of the external fields are less than the self-widths of the lines by 10^{-2}–10^{-6} and give rise to only negligibly small broadenings of the lines.

In the electron rings the ions are formed as a result of electron collisions with neutral atoms or molecules of the residual gas. The initial energy of the ions is equal to the energy of the neutral atoms and is lower by several orders of magnitude than the electric potential of the ring. The produced ions begin to execute oscillatory motions in the small cross section of the ring and are subject to further ionization. In principle, the magnetic field at right angles to the plane of the ring, collisions with electrons, and other factors may cause longitudinal motion of the ions, i.e., azimuthal motion around the ring. Motion of the ions in the ring leads to Doppler broadening of the measured lines.

Let us consider the broadening of the lines due to transverse oscillations of the ions in the case of observation through a collimator situated in the plane of the ring (Fig. 12). The electrons in the section of the ring have a nonuniform density, which can be best described by a Gaussian distribution:

$$\rho_e(r) \sim \exp(-r^2/2a_e^2).$$

To such an electron distribution there corresponds at small neutralization factors f the ion density [24,82]

$$\rho_i(r) \sim \exp(-r^2/2a_i^2)/r, \tag{4}$$

where $a_i^2 = a_e^2/2I$, and the mean-square velocity of the oscillations of the ions is almost independent of the charge state of the ions:

$$\overline{v_i^2} = \omega_i^2 a_i^2 \approx \omega_1^2 a_1^2 \approx \text{const}. \tag{5}$$

The characteristic frequency ω_i of the ion oscillations is determined from

$$\omega_i^2 = \frac{1}{1836}\frac{I}{A}\frac{N_e}{2\pi R}\frac{r_0 c^2 a_i^2}{a_e^2 + a_i^2}(1-f), \tag{6}$$

where $r_0 = e^2/mc^2$ is the classical radius of the electron, A is the mass number of the ions, and a_e and a_i are the radii of the

TABLE I. Typical strengths of the electric and magnetic fields that act on ions, compared with the field strengths in atoms.

Type of field	Field strengths		Line broadening
	in atom	in compression chamber	
Magnetic	$\frac{v_e}{\mu_0 c^2} \mid E \mid \approx 10^6$ A/m	$\mid H \mid \approx 10^6$ A/m	$\approx 10^{-4}$
Electric	$\frac{e}{4\pi\varepsilon_0 a_0^2} \approx 5\cdot 10^{11}$ V/m	$\mid E \mid \approx 2\cdot 10^8$ V/m	$\approx 10^{-3}$

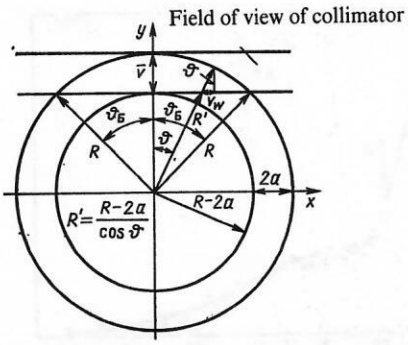

FIG. 12. Geometry of collimator near an electron–ion ring.

cross sections of the electron and ion rings. Hence, for $I \gg 1$, we obtain

$$\bar{v}_i^2 = \frac{1}{1836} \frac{r_0 c^2}{A} \frac{N_e}{2\pi R} (1-f). \tag{7}$$

For $N_e = 10^{13}$ and $R = 2$ cm, ions of the element Xe move with mean velocity

$$\bar{v}_{Xe} = 2 \cdot 10^7 \text{ cm/sec}.$$

From Fig. 12 we can calculate the component of the velocity $\bar{v}_C$ of the ions in the direction of the collimator, averaged over the field of view of the collimator:

$$\bar{v}_C = \frac{\bar{v}_i}{\pi \vartheta_G} \frac{2a}{R}, \tag{8}$$

where $\vartheta_G = \cos^{-1}[R - a/R]$ is the limiting angle of the field of view of the collimator. For $a = 0.15$ cm, we obtain ϑ_G 23.9° and $\bar{v}_{C,Xe} \approx 2.3 \times 10^6$ cm/sec. The broadening ΔE of an x-ray line of energy E_x due to the Doppler effect is

$$\Delta E = 2 \frac{\bar{v}_C}{c} E_x \cos\varphi, \tag{9}$$

where φ is the angle between the direction of motion of the source of the radiation and the direction of observation.

For these conditions, the line broadening is found to be

$$\Delta E = 5.4 \cdot 10^{-4} \frac{E_x}{\vartheta_G} \sqrt[4]{\frac{I(1-f)^2}{A^2}} \tag{10}$$

and

$$\Delta E_{max} = 1.3 \cdot 10^{-3} E_x \sqrt[4]{\frac{I}{A^2}}, \tag{11}$$

and for the conditions given above and for xenon ions this gives

$$\Delta E_{max} (K_\alpha - Xe^{5+}) \approx 5 \text{ eV}. \tag{12}$$

In Table II we compare the maximal Doppler broadenings of the K_{α_1} and L_{α_1} lines of some ions with their natural widths. It can be seen that the contribution of the Doppler effect to the total width of the emission lines in the case of observation of only the upper part of the ring (Fig. 12) is about 30–50% for light ions and 15–20% for heavy ions.

The line broadenings for singly charged ions take values at the level 30–50% of the maximal values and thus make a small contribution to the total width. On the other hand, if the complete electron–ion ring is observed simultaneously, the line broadenings are an order of magnitude greater than (9) and become comparable with the natural widths ω_λ. This makes it significantly harder to resolve the x-ray lines of the neighboring degrees of ionization.

The need to limit the Doppler broadening of the lines reduces the total observed intensity of the characteristic x rays of the ions in electron–ion rings. Collimation of the investigated radiation leads to a lowering of the efficiency of exploitation of the ring as a source by a factor

$$T = \vartheta_G/\pi, \tag{13}$$

which under real conditions takes values $T \approx 0.1$. The number of x rays of a certain line detected during a time interval τ can be estimated by the formula[31]

$$N_x = \sigma_{nlj} N_i N_e \frac{v_e \tau}{2\pi^2 a^2 R} \omega_{nlj} S T, \tag{14}$$

where σ_{nlj} is the cross section for ionization of the subshell with quantum numbers (nlj), ω_{nlj} is the probability of radiative decay of the excited ion with emission of a photon of the observed line, S is the luminosity of the measuring instrument,

$$S = \frac{\Delta\Omega}{4\pi} \eta e^{-\mu x}, \tag{15}$$

where $\Delta\Omega$ is the detection solid angle, η is the efficiency of detection of the instrument at the energy of the observed radiation, and $\mu = \mu(E_x)$ is the total coefficient of absorption of the radiation in the materials through which it has passed. For an estimate, we take as an example xenon, so that

$$\sigma_{101/2} = 5 \cdot 10^{-23} \text{ cm}^2;$$
$$\omega_{101/2} = 0.9.$$

One can estimate the necessary value of the product of S of the instrument and the ring lifetime τ,

$$S\tau \geqslant N_x \cdot 2.2 \cdot 10^{-12}, \tag{16}$$

if N_x x rays are to be observed during a cycle in the compression chamber. For the acceleration regime, the collective heavy-ion accelerator KUTI-20 has $\tau = 500\ \mu$sec and

TABLE II. Comparison of the maximal Doppler broadenings of K_{α_1} and L_{α_1} lines of some ions with charge I and their natural widths ω_λ.

Ion	$I = Z-1$	$\omega_\lambda(K_{\alpha_1})$, eV	ΔE, eV	$\omega_\lambda(L_{\alpha_1})$, eV	ΔE, eV
$_{18}$Ar	17	0.8	1.2	0.1	0.09
$_{36}$Kr	35	3.9	4.4	1.2	0.5
$_{54}$Xe	53	14.6	9.1	3.1	1.2
$_{79}$Au	78	57.4	18.9	5.4	2.7
$_{92}$U	91	103.5	25.6	7.4	3.5

$$S \geqslant N_x \cdot 4.4 \cdot 10^{-9}, \tag{17}$$

and for the compression-chamber regime with specially lengthened ring confinement time $\tau = 30$ msec

$$S \geqslant N_x \cdot 7.3 \cdot 10^{-11}. \tag{18}$$

The proportionality $N_x \sim \tau$ also justifies the requirement of an increase of the ring lifetime from the point of view of the effectiveness of using electron–ion rings as sources for investigating the characteristic x-ray emission of highly charged ions.

3. USE OF THE CRYSTAL-DIFFRACTION METHOD FOR X-RAY SPECTROMETRY OF HIGHLY CHARGED IONS

The conditions for spectrometric measurements of the characteristic x rays of highly charged ions in different types of ion sources (electron–ion rings, electron-beam sources, laser ion sources, plasma sources based on electron-cyclotron resonance, stripping of ions in beams of heavy-ion accelerators, production of highly charged ions in energetic ion–atom collisions, etc.) do not in principle differ very much:

a) usually, the object of investigation is an ensemble of highly charged ions with a definite distribution of the ions over several degrees of ionization I (see Sec. 1);

b) the charge dispersion ΔI is a few units;

c) the conditions of excitation of the x-ray states for the different ion charges are similar;

d) the spectra of the characteristic x rays are complicated because of the existence of the dispersion ΔI;

e) the intensity of the characteristic x rays is moderate;

f) detection of the radiation is possible in relatively small solid angles.

On the basis of this, we can formulate general requirements on the method of measurement:

a) a high energy resolution of the spectrometer to identify the lines of high-charge states of the ions;

b) a high luminosity of the spectrometer to optimize the efficiency of the measurements:

c) a high stability of the apparatus during fairly long measurement times.

The restriction on the possibility of spectrometry by means of semiconductor detectors is illustrated in Fig. 13. The widths of the measured lines are determined by the resolution of the spectrometer. They greatly exceed both the natural widths of the x-ray transitions and the energy splitting of the fine structure. The investigation of the satellite lines that correspond to different distributions of the vacancies in the electron shells and appear in the form of additional structures in the spectra encounters great difficulties and can be achieved by means of semiconductor detectors only "inclusively."

The highest resolution and precision in the energy range of the x-ray transitions of ions is achieved by a crystal-diffraction spectrometer (CDS).[31,41] This exploits the diffraction of x rays by the crystal planes of single crystals. The occurrence of diffraction peaks satisfies the Bragg law

$$n\lambda = 2d \sin \vartheta_n, \tag{19}$$

where d is the interplane separation of the crystal lattice, ϑ_n is the Bragg angle, and n is the order of the diffraction maximum. The one-to-one relationship between the Bragg angle and the wavelength makes it possible to determine the energy of the x-ray lines

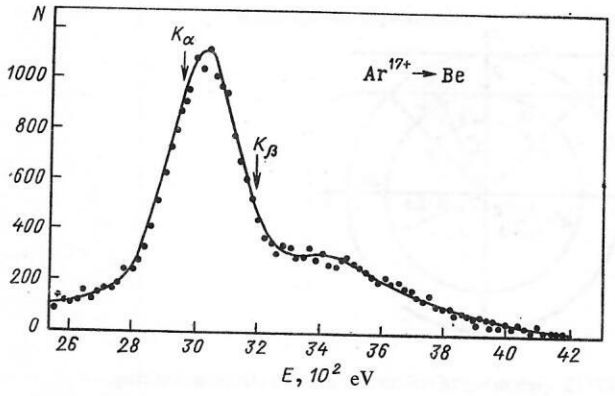

FIG. 13. Spectrum of neutralization radiation of argon in the $Ar^{17} \rightarrow Be$ reaction, obtained by means of a hyperpure Ge detector.

$$E_x = \frac{ch}{\lambda} \tag{20}$$

(c is the speed of light in vacuum, and h is Planck's constant) by accurate measurement of the angle ϑ_n. The accuracy in the determination of λ is

$$\left|\frac{\Delta\lambda}{\lambda}\right| = \cos\vartheta\,\Delta\vartheta \tag{21}$$

and depends only on the angle ϑ and its displacement $\Delta\vartheta$ if we ignore the temperature dependence

$$\Delta d = \alpha \Delta T, \tag{22}$$

where α is the coefficient of expansion of the crystal, and T is its temperature.

The accuracy in the determination of the energy also depends on the errors in the determination of the fundamental constants,[42]

$$\left|\frac{\Delta E}{E}\right| = \left|\frac{\Delta\lambda}{\lambda}\right| + \left|\frac{\Delta(ch)}{ch}\right|, \tag{23}$$

which, because they are small compared with the other errors, will be ignored in what follows. From the Bragg law (19) we obtain the dynamical range of measured λ for a definite analyzing crystal:

$$\left.\begin{aligned} &\lambda_{\max}\,(\widehat{=} E_{\min}) < 2d; \\ &\lambda_{\min}\,(\widehat{=} E_{\max}) = 2d\vartheta_{\min}, \end{aligned}\right\} \tag{24}$$

where $\vartheta_{\min}$ is the minimal realized angle of the spectrometer (usually about 5°). Since the angular dispersion of the decomposition by the crystal of the radiation into the spectrum,

$$\frac{\Delta\vartheta}{\Delta\lambda} = \frac{n}{2d\cos\vartheta_n}, \tag{25}$$

decreases with increasing ϑ_n (Fig. 14), the resolution of the crystal-diffraction spectrometer also decreases. This also follows from (21) and may lead to additional restrictions on the useful dynamical range. Although the angular dispersion and $E_{\max}$ are greater for the higher orders n, the reflectivity of the crystals decreases at the same time (Fig. 15, Ref. 43). This reduces the ratio of the measured effect to the background and reduces the efficiency of measurement. Therefore, the use of the crystal-diffraction method for sys-

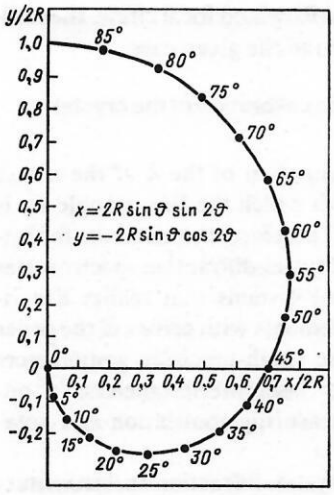

FIG. 14. Trajectory of motion of detector in a crystal-diffraction spectrometer: ϑ is the Bragg angle, and R is the radius of the focal circle. The curve is for the technical solution of the kinematics of the spectrometer that permits one to maintain the direction from the source to the crystal in the process of measurement, this being a necessary condition for operation with fixed external sources of radiation.

tematic investigations necessarily requires the presence of a definite set of analyzing crystals that realize different values of d.

A comparison of the resolutions of a crystal-diffraction spectrometer and a semiconductor detector is modeled in Fig. 16 for the L_{α_1} lines of the ions Kr^{8+}–Kr^{12+}. It can be seen that the structure of the total line, measured by the semiconductor detector, can be resolved by the crystal-diffraction spectrometer if it is assumed that the measurement is made at sufficiently large ϑ. This can be realized, for example, by using a SiO_2 $(10\bar{1}0)$ crystal. Figure 16 does not show the L_{α_2} lines, which are shifted relative to the L_{α_1} lines by distances comparable to the natural widths; this additionally complicates the picture. The decomposition of such spectra into individual components by means of mathematical fitting procedures depends strongly on the statistics.[44] In addition, it is necessary to make definite analytic assumptions about the shape of the measured lines, and this often does not correspond to the physical picture of the process of measurement by the crystal-diffraction method because of the complexity of the instrumental curves of the spectrometer.[45,46]

However, the range of variation of the required parameters of the lines in the spectra can be significantly limited on the basis of modern computational data on the shifts of the x-ray lines as functions of the degree of ionization.[36] The process of analysis of the complicated diffraction Spectrum should then be done in accordance with a scheme of the following type:

a) modeling of the instrumental curve of the crystal-diffraction spectrometer in the region of angles ϑ at which the measurements are made and for definite parameters of the facility in the chosen geometry by the methods indicated in Refs. 45 and 46;

b) restoration of the measured spectrum, i.e., recovery of the emission spectrum of the source undistorted by the process of measurement;

c) decomposition of this spectrum into individual components with definite assumptions about the shape of the lines, their energy positions in the spectrum, etc.

The possibility of systematic analysis of the diffraction spectra of the characteristic x rays of the ensemble of highly charged ions in accordance with this basic scheme must still be subjected to a detailed investigation. The method of analysis becomes complicated if the spectrum consists of many components of different intensities near each other, and if the statistics of the measured spectrum is poor. Such a situation is expected for insufficiently highly ionized atoms. In such a case one can determine only the averaged values over the complete ion ensemble.

The choice of the Bragg or von Laue scheme for the crystal-diffraction spectrometer must be made with simultaneous allowance for the energies of the x-ray lines of the investigated ions and their natural widths as functions of Z and I. As was shown in Sec. 1, high charge states are attained in electron–ion rings for light and medium Z, where the energy of the K transitions lies in the interval of about 1–20 keV. This range also includes the L lines of the medium and heavy ions and M lines of the heavy ions. Bearing in mind the behavior of the natural widths of these lines (see Fig. 5) with variation of Z, it is expedient to choose the reflection form of crystal-diffraction spectrometer of Bragg type.

A high angular dispersion can be achieved using the more complicated planes of LiF and SiO_2 crystals with small interplane spacings $d \approx 0.1$ nm. However, for crystals with

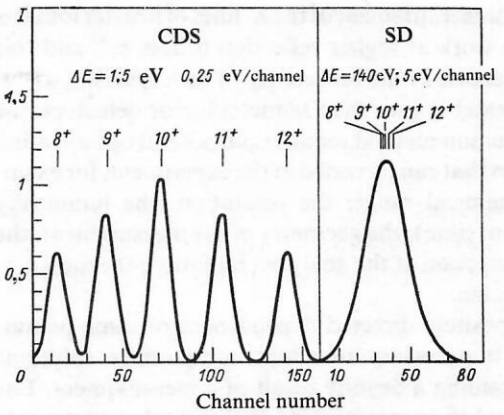

FIG. 16. Comparison of resolutions of a crystal-diffraction spectrometer (CDS) and a semiconductor detector (SD) for the example of an ion ensemble from Kr^{8+} to Kr^{12+} for the L_{α_1} line and $\Delta\omega = 3$ eV (ΔE is the energy resolution of the spectrometer).

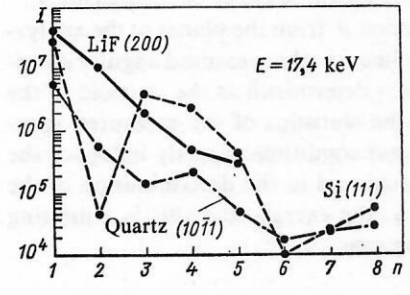

FIG. 15. Dependence of the intensity I of x-ray reflections on the reflection order n for x-ray energy 17.4 keV (Mo–K_α) for LiF(200) quartz $(10\bar{1}1)$, and Si (111) (Ref. 43).

large d and for measurement of the K lines of heavier ions it is necessary to work at higher reflection orders n,[43] and this leads to a decrease in the reflectivity of the crystals.

To a greater degree than semiconductor detectors, the crystal-diffraction method requires purposeful optimization of parameters that can be varied in the experiment, for example: the dynamical range; the resolution; the luminosity (measurement time); the geometry of the measurement; the method of detection of the analyzed radiation; the measurement regime, etc.

The oppositely directed dependences of some parameters make it necessary to adopt compromise solutions aimed at obtaining a definite result of a measurement. For example, to use the procedure for analyzing the spectra it is necessary to have a definite event statistics[44] in order to obtain the properties of the spectra (the positions and half-widths of the lines) with the necessary "mathematical" accuracy. However, a high resolution can be achieved only by limiting the luminosity and, thus, increasing the measurement time.

We shall discuss further the use of the crystal-diffraction method in the case of a focusing crystal-diffraction spectrometer of Bragg type for investigation of the spectra of the characteristic x-ray radiation of highly charged heavy ions.

4. PROPERTIES OF A FOCUSING CRYSTAL-DIFFRACTION SPECTROMETER OF BRAGG TYPE

In 1984 a focusing crystal-diffraction spectrometer in the geometry of Johansson (Fig. 17) was commissioned at the JINR. It can work in the range of angles $7 \leqslant \vartheta \leqslant 70°$.[32] The instrument is completely automated and controlled by a program with a minicomputer.[47,48] The technical resolution of the kinematics of the crystal-diffraction spectrometer makes it possible to maintain the direction from the source to the crystal when the angle ϑ is varied (see Fig. 14);[49] this is a necessary condition for operating with "external" fixed sources of radiation (ion sources, accelerators, etc.). The entry slit is displaced along a straight line, while the detector slit executes a synchronous motion along a cycloid in order to fulfill the condition for focusing for any ϑ in the indicated range. This means that both slits and the surface of the concave crystal are always on the Rowland focal circle, the radius of which is $R_F = 324$ mm in the given case.

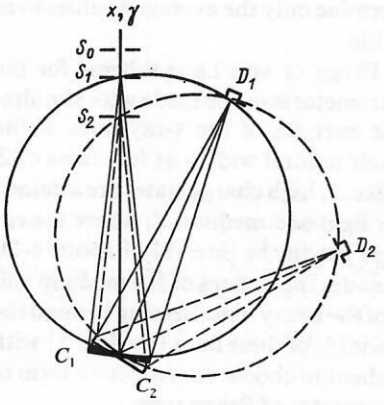

FIG. 17. Focusing crystal-diffraction spectrometer in Johansson geometry (Refs. 25 and 26): S is the diaphragm, C is the crystal, and D is the detector. The indices 1 and 2 indicate different positions of the elements for different Bragg angles.

Accuracy of measurement and calibration of the crystal-diffraction spectrometer

The accuracy of determination of the λ of the x rays depends on the accuracy with which the Bragg angle ϑ_n is set and on its repeatability. Therefore, the elements for setting and measuring ϑ in the crystal-diffraction spectrometer are precision optomechanical systems that realize a variation of the position of the elements with errors of the order of 1 μm or one second of arc (high-precision goniometers with step drives, piezodrives,[50] laser interferometers,[51,52] optomechanical devices for measuring translation and rotation[53,54]).

By means of focusing crystal-diffraction spectrometers one can make a relative measurement of the wavelength λ of the characteristic x rays. To calibrate the spectrometer, one needs a set of standard (reference) lines λ_i, which must be measured under geometrical conditions identical to those of the subsequent measurement in order to avoid systematic errors. As a rule, for this one requires an auxiliary apparatus, for example, an x-ray tube to excite fluorescence lines.

In the general case, the calibration curve $\lambda = f(\vartheta)$ can be represented in the form

$$f(\vartheta) = a_0 + a_1 \sin\vartheta + a_2\vartheta^2 + a_3\vartheta^3 + \ldots, \qquad (26)$$

where [apart from the second term, which follows from the law (19)] allowance is made for some corrections associated with instrumental effects (for example, aberration). Then the coefficients a_i are determined by means of the reference lines λ_i. In actual fact, the angle ϑ is measured relative to some zero position ϑ_0, i.e., $\vartheta = \vartheta_0 + \delta\vartheta$, and ϑ_0 appears as an additional unknown parameter in (26).

The calibration procedure was investigated in Ref. 51 for the case when the angle ϑ is measured by a laser interferometer. Corrections arise in this case because of the tolerances of the optical elements. After determination of the coefficients a_i of the calibration curve, one can, by a compensating calculation, find improved values of the measured sin ϑ. The error in these values then depends only on the errors in the reference lines. However, one needs about twice as many calibration lines as there are coefficients to be determined. Therefore, the expediency of constructing a function of the type (26) was investigated in Ref. 55. It was found that there is a correlation between the coefficients for definite powers of the angle ϑ in (26) and the result of the calibration. This made it possible to separate the principal correction terms and reduce the number of coefficients a_i.

The angle of reflection ϑ from the planes of the analyzing crystal for a certain line λ in the measured angular distribution of the spectrum is determined as the centroid of the reflection. Therefore, the statistics of the measured spectrum and the background conditions directly influence the accuracy that can be achieved in the determination of the position of the line, i.e., the energy, and this is a limiting factor at a low counting rate.

Geometrical aberrations

We consider in more detail the process of measurement with a crystal-diffraction spectrometer. If we know all the

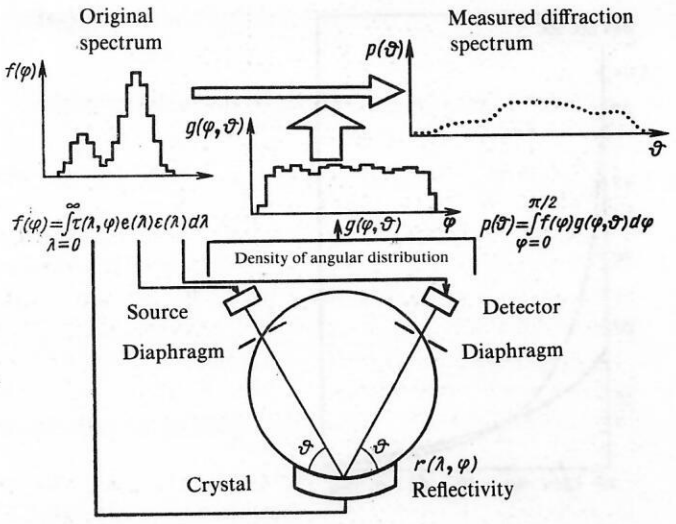

FIG. 18. Influence of the geometry of the experiment and properties of the spectrometer on the result of measurement.[46]

geometrical dimensions of the elements of the spectrometer and the source (for example, the distances, slit widths, measurements of crystal, radius R_F, etc.); if the radiation source of the spectrum $e(\lambda)$ is known; if we have determined the wavelength λ of the radiation that passes through the entry slit of the spectrometer and impinges at angle φ on the crystal surface of the analyzer and it is also known that the condition (19) between φ and λ is satisfied, i.e., the x ray is reflected by the crystal in accordance with its reflectivity; and if the reflected radiation passes through the detector slit and is detected by a counter with efficiency $\epsilon(\lambda)$—then the probability of detecting events for setting angle ϑ of the spectrometer can be represented in the form[56]

$$p(\vartheta) = \int_{\varphi=0}^{\pi/2}\int_{\lambda=0}^{\infty} g(\varphi, \vartheta)\, \varepsilon(\lambda)\, e(\lambda)\, r(\lambda, \varphi)\, d\lambda d\varphi, \qquad (27)$$

as is demonstrated in Fig. 18. The geometrical factor $g(\varphi,\vartheta)$ represents the distribution of all possible realized reflection angles φ for a definite fixed setting angle ϑ of the spectrometer. It gives rise to a distortion of the spectrum, i.e., the shape of the lines, in the process of measurement due to the finite sizes of the elements of the spectrometer (geometrical aberrations).

The influence of the function $g(\varphi,\vartheta)$ on the attainable resolution of a focusing crystal-diffraction spectrometer was investigated in Ref. 46 by the method of statistical modeling. Phenomena associated with the crystal structure and processes of extinction and absorption of the radiation were ignored. Then the expression (27) simplifies to

$$p(\vartheta) = \int_{\varphi=0}^{\pi/2} g(\varphi, \vartheta)\, f(\varphi)\, d\varphi \qquad (28)$$

and is the convolution of the measured spectrum $f(\varphi)$ at angle ϑ with a certain geometrical response function $g(\varphi,\vartheta)$.

A program VERDI[46] was used to model the distributions $g(\varphi,\vartheta)$ for definite conditions of measurement for ϑ equal to 20, 40, 60, and 80° (Fig. 19). The shifts of the centroids of the distributions of φ_s with respect to the spectrometer setting angle ϑ and the variance of $\delta\varphi_s$ were calculated; H was determined as the geometrical efficiency of event detection.

Figure 20 shows the dependences of $\varphi_s, \delta\varphi_s H$ on the

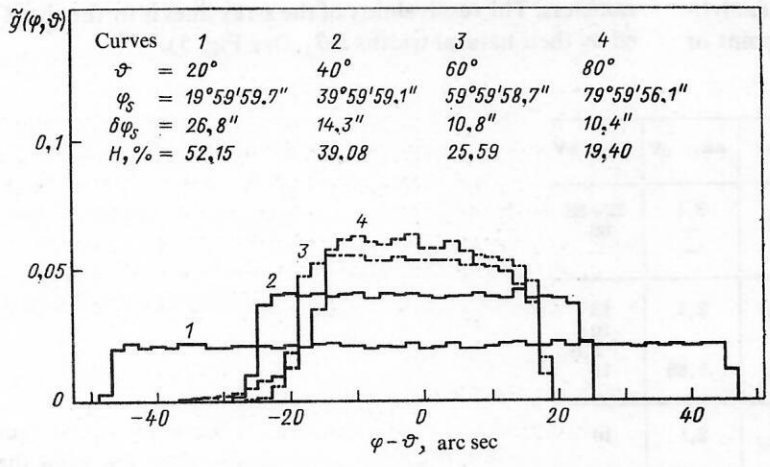

FIG. 19. Modeling of the geometrical function $\tilde{g}(\varphi,\vartheta)$ of the Dubna crystal-diffraction spectrometer for different angle positions ϑ of the spectrometer. The detector diaphragm and the entry diaphragm were taken to measure 0.1×10 mm and for the crystal 10×40 mm, while the radius of the focal circle was 324 mm. The shape of the source is a rectangle measuring 0.1×10 mm placed outside the focal circle.

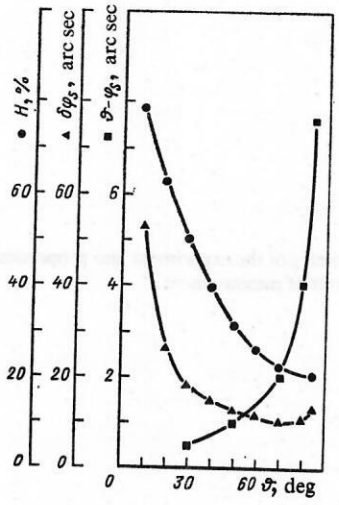

FIG. 20. Dependence of φ_s, $\delta\varphi_s$ and H on the angle ϑ. For the parameters of the spectrometer, see the caption to Fig. 19.

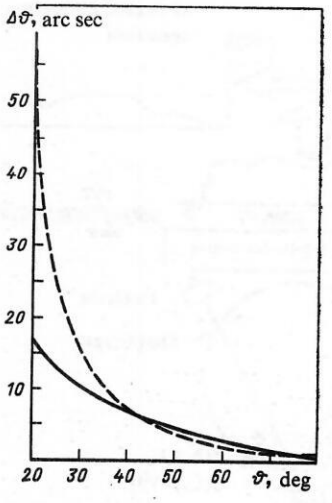

FIG. 21. Dependences of the geometrical widths $\Delta\vartheta$ of the diffraction reflections on the spectrometer setting angle ϑ for a focusing crystal-diffraction spectrometer of Johansson type with radius $R_F = 100$ mm of the focal circle. The continuous curve corresponds to a flat crystal, and the broken curve to a focusing crystal.

angle ϑ. It can be seen that the shifts of the reflections are large at large angles. To the unit of angle in Fig. 20 there corresponds an energy interval of the order 0.1 eV at small ϑ and 0.01 eV at large ϑ for the existing spectrometer with SiO_2 $(13\bar{4}0)$ crystal.

The variances of the distributions $g(\varphi,\vartheta)$ increase with decreasing ϑ. Since the width of a measured reflection is related to the width of the distribution $g(\varphi,\vartheta)$ (28), there is a restriction on the resolution that can be achieved by the spectrometer.

As an example, Fig. 21 shows the dependences of the geometrical widths of the diffraction reflections on the setting angle ϑ for a focusing crystal-diffraction spectrometer of Johansson type with radius $R_F = 100$ mm of the focal circle. As another crystal, quartz SiO_2 $(13\bar{4}0)$ was also chosen. It can be seen that in the region of angles $\vartheta \leqslant 30°$ the reflections are broad, and, therefore, the resolution there is less good.

Hitherto we have regarded the diffraction of x rays by the crystal planes as a process that satisfies the laws of geometrical optics. This approach has enabled us to identify purely geometrical effects and investigate their influence on the resolution of the spectrometer separately. In real measurements with focusing crystal-diffraction spectrometers these are indeed often the dominant effects.

The geometrical aberrations of crystal-diffraction spectrometers with concave crystals were investigated analytically in Refs. 45, 57, and 58 under conditions of point or small sources placed on the focal circle. This idealization makes it possible to use certain approximations in the derivation of the expressions that relate the aberration effects to the parameters of the instrument, and this makes it possible to optimize instruments and compare their integrated parameters (for example, the energy resolution, luminosity, etc.).

Resolution of crystal-diffraction spectrometers

The width of the instrumental curve of a crystal-diffraction spectrometer and the associated possibility of resolving the x-ray lines can be estimated by using the expression (21) in the form

$$\Delta\lambda = \lambda \operatorname{ctg}\vartheta\Delta\vartheta. \tag{29}$$

The angle displacement $\Delta\vartheta$ consists of several terms:[59,60]

$$\Delta\vartheta = \Delta\vartheta_{cr} + \Delta\vartheta_A + \Delta\vartheta_\lambda, \tag{30}$$

where $\Delta\vartheta_{cr}$ is the contribution from the crystal structure, in practice a quality parameter of the material of a mosaic crystal; $\Delta\vartheta_A$ is the line broadening due to the finite size of the elements of the spectrometer (the geometrical aberrations were considered above); $\Delta\vartheta_{cr} + \Delta\vartheta_A$ are instrumental parameters. The resolvability of the x-ray lines is further limited by their natural widths $\Delta\vartheta_\lambda$ (see Fig. 5).[61,62]

TABLE III. Typical mosaic effects of some crystals.[58,62]

Crystal plane	2d, Å	Γ	$\Delta\vartheta_{cr}$, 10^{-4} rad	X-ray line	ΔE_λ, eV	ΔE_K, eV
LiF (200)	4,0276	0.2	5—20	Br—K_{α_1}	3,4	22—88
(220)	2,84	0.1	20		—	60
(420)	1.79	—	—		—	—
SiO_2 (1010)	8.50967	—	—	Cu—K_{α_1}	2,1	13
(1011)	6,68637	0,5	3			10
(1340)	2,36013	—	—			2,8
(5052)	1,624	—	—	Mo—K_{α_1}	5,86	11
Ge (111)	6,532	0,7	3	Cu—K_{α_1}	2,1	10

TABLE IV. Energy resolution ΔE and total efficiency ϵ of various spectrometers for selected x-ray energies.[29]

Детектор	Parameter	Energy of x rays, keV		
		10	50	100
Hyperpure germanium HPGe	ΔE, eV ε	190 $1.8\cdot10^{-3}$	300 $2.0\cdot10^{-3}$	400 $8.0\cdot10^{-4}$
Ge (Li) 1 cm^3	ΔE, eV ε	270 $1.8\cdot10^{-3}$	360 $2,0\cdot10^{-3}$	475 $8.0\cdot10^{-4}$
Si (Li) 30 $mm^2\times4mm$	ΔE, eV ε	180 $1.8\cdot10^{-3}$	— $3.8\cdot10^{-4}$	— $2.4\cdot10^{-5}$
NaI (Tl) 7,62×7,62 cm	ΔE, keV ε	— —	2 $1,0\cdot10^{-1}$	4,5 $8,0\cdot10^{-2}$
CDS	ΔE, eV ε	8 $4,0\cdot10^{-6}$	30 $3.0\cdot10^{-7}$	200 $6.0\cdot10^{-8}$

For some crystal analyzers, Table III gives typical values of the mosaic term.[58,62] The broadenings ΔE_{cr} of the chosen lines due to these quantities are compared with the natural widths ΔE_λ. We also give the doubled interplane separation $2d$ and the reflection coefficient Γ for the first order, $n = 1$ [see (19)].

The flux intensities for the higher reflection orders and crystal planes of the materials often used as analyzers, for example, SiO_2, LiF, Ge, Si, etc., were investigated in Ref. 43. The reflectivities of the crystals were calculated by means of the program PBRAGG,[63] and the results of the calculations were compared with data obtained experimentally. Generalizing the results, we may conclude that the reflection intensities at the higher reflection orders $n = 2, 3, 4, 5,...$ for crystals such as LiF and quartz decrease almost monotonically with increasing n, while the crystals Si and Ge are characterized by a nonmonotonic dependence of the reflectivity on n. Minima are observed for n equal to 2 and 6 and maxima for n equal to 3, 4, and 5, the difference between a minimum and a maximum reaching values of the order of 10^2 (Refs. 43 and 63). Bearing in mind that the angular linearly on the reflection order n [see (25)], it may in certain situations be advantageous to work at higher n, gaining in resolution at the expense of a certain loss in intensity.

Luminosity

In Table IV (Ref. 29) we give typical values of the energy resolution and efficiency of various x-ray detectors in the energy range from 10 to 100 keV, which is of interest for the spectrometry of the x rays of highly charged ions. Figure 22 shows the relative efficiencies for detection of various semiconductor detectors, Fig. 23 shows the relative efficiencies of proportional and scintillation counters, and Fig. 24 shows the relative energy resolution of various detectors as a function of the energy of the radiation incident on the detector. It is obvious that measurement of soft x rays is particularly complicated, since for this one requires very thin detector windows with a high transmission coefficient and especially thin dead layers of the detector.

Comparing the parameters of the crystal-diffraction spectrometers with semiconductor detectors, we see that the improvement in the resolution by 1–2 orders of magnitude is accompanied by a decrease in the efficiency by three orders of magnitude or more. The experimental situation can be uniquely characterized by the luminosity parameter S of the

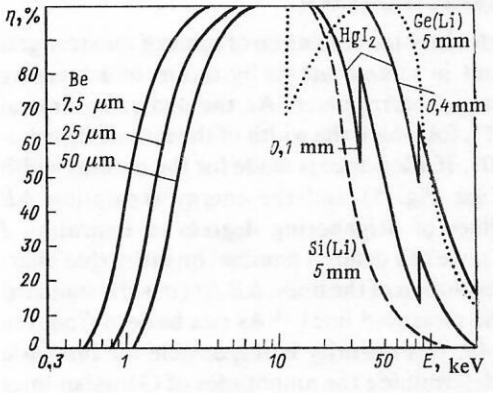

FIG. 22. Dependence of the detection efficiency η of semiconductor detectors on the radiation energy E. The figure shows the type of semiconductor detector, the thickness of the detector, and, for low energies, the limiting energy that can be measured, determined by the absorption of the radiation in the Be windows of the detectors of different thicknesses.

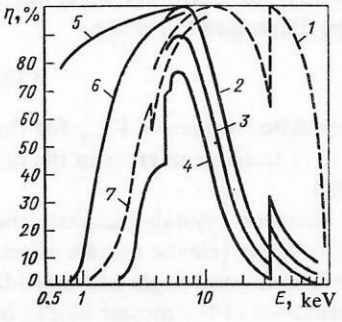

FIG. 23. Dependence of the detection efficiency η on the radiation energy E: 1) scintillation counter NaI(Tl) of thickness 10 mm; 2) proportional counter filled with Xe/CH_4 with pressure $p = 760$ mm Hg; 3) proportional counter filled with Xe/CH_4 with $p = 500$ mm Hg; 4) proportional counter filled with Xe/CH_4 with $p = 300$ mm Hg; 5) absorption of radiation by mylar of thickness $t = 1$ μm; 6) absorption of radiation by mylar with $t = 5$ μm; 7) absorption by mica with $t = 5$ μm.

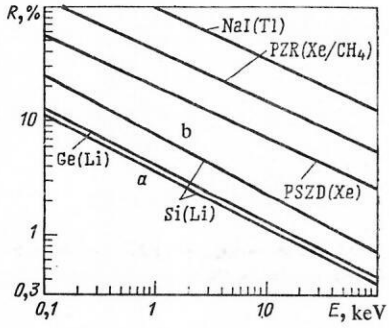

FIG. 24. Relative energy resolution R of various detectors as a function of the radiation energy E: PZR, proportional counter filled with Xe/CH_4; PSZD, proportional–scintillation counter filled with Xe; Si(Li), practical range of resolution of Si(Li) detector; a) with liquid-nitrogen cooling; b) with thermoelectric cooling.

instrument, which is defined as the ratio of the number of events detected by the spectrometer to the number of x rays emitted by the source.

In Ref. 64 the spectrometer luminosity was defined by the expression [see (15)]

$$S=\frac{\Delta\Omega}{4\pi}\frac{R_i}{\omega}\varepsilon_D e^{-\mu x}, \tag{31}$$

where $\Delta\Omega$ is the effective solid angle of reflection of the analyzer crystal, R_i is the integrated reflectivity of the crystal, ω is the width of the diffraction reflection, ϵ_D is the counter detection efficiency, and μ is the linear absorption coefficient of the radiation in the materials. Under the assumption that the diffraction line can be approximated by a Gaussian distribution—this is the case for mosaic crystals—determination of the reflection coefficient Γ,[58]

$$\Gamma = R_i/\omega,$$

where

$$R_i=\int_{-\infty}^{+\infty}\frac{I(\varphi)}{I_0}d\varphi, \tag{32}$$

amounts to averaging the integrated reflectivity over the width of the reflection if $I(\varphi)/I_0$ is the ratio of the intensity of the radiation reflected by the crystal at angle φ to the intensity I_0 of the radiation incident on the crystal at angle ϑ. Then the maximum of the diffraction line will be

$$\Gamma_{\max} = \Gamma/1{,}07. \tag{33}$$

Therefore, the use of the tabulated values of $\Gamma_{\max}$ for the reflection coefficient[58,65] in (31) leads to an error in the determination of S of order 10%.

Elastic bending of the focusing crystals increases the mosaic effect relative to flat crystals (elastic mosaic effect; see Ref. 58). The effective reflection solid angle $\Delta\Omega$ depends on the width ω_{cr} of the distribution of the mosaic blocks of the crystal. In the case of a small entry diaphragm of the focusing crystal-diffraction spectrometer, we have

$$\Delta\Omega = \Delta\alpha\Delta\beta, \tag{34}$$

where $\Delta\alpha$ and $\Delta\beta$ are the maximal admissible horizontal and vertical divergences of rays reflected by the crystal. Since

$$\Delta\alpha=\omega_{cr};\quad \Delta\beta=2\sqrt{\omega_{cr}\operatorname{ctg}\vartheta}, \tag{35}$$

it follows that for each setting angle ϑ of the spectrometer there exists a definite reflection zone on the analyzing crystal. Rays that have wavelength λ corresponding to the angle ϑ can be reflected by the crystal when they are incident on this zone. However, the weights with which the individual small elements of this zone make their contribution to the total event count are not the same but depend on their illumination and on the direction of the mosaic blocks. It must be emphasized that $\Delta\Omega$ is not identical to the geometrical aperture of the crystal and depends on the angle ϑ. Therefore, the luminosity of the spectrometer is also a function of the angle, i.e., $S=S(\vartheta)$, and it is therefore correlated with the energy of the investigated radiation.

The reflection zones were calculated analytically under the assumption that monoenergetic x rays incident on the crystal can be deflected from the angle ϑ by $\pm\omega_{cr}/2$. The same result was obtained by statistical modeling of the function $g(\varphi,\varphi)$,[66] when a raster of events reflected from the crystal was formed corresponding to small angle intervals $\delta\varphi_i=\varphi_i-\varphi_{i-1}$ near the setting angle ϑ. In this case the weights of the elements of the reflection zone are automatically obtained as the ratio of the number of events from rays reflected in the interval $\delta\varphi_i$ to the total number of events.

Both approaches are limiting cases and complement each other, since monoenergetic radiation never occurs in nature, and in real experiments there is neither a point source nor geometrical reflection of radiation from a crystal. Analysis of the resolution of two closely spaced x-ray lines for specific experimental conditions of measurement with focusing crystal-diffraction spectrometers and the exact determination of the spectrometer luminosity are therefore nontrivial problems. The factorization of the spectrometer response function (27) indicates distortion of the measured spectrum $p(\vartheta)$ relative to the source spectrum $e(\lambda)$ in both shape and intensity. Therefore, the reliable recovery of the spectrum $e(\lambda)$, particularly when it is complicated, from $p(\vartheta)$ requires further attention.

5. MEASUREMENT OF CHARACTERISTIC X RAYS OF HIGHLY CHARGED HEAVY IONS WITH A FOCUSING CRYSTAL-DIFFRACTION SPECTROMETER

We consider here the resolution of some of the strongest x-ray transitions in ionized atoms by means of a focusing crystal-diffraction spectrometer. As the analyzing crystal we take Si(111), for which the width of the mosaic distribution is $\omega_{cr}\approx 10''$. If allowance is made for the natural width of the lines (see Fig. 5) and the energy separation ΔE between the lines of neighboring degrees of ionization I (Figs. 6 and 8), we can define a nominal quantity that characterizes the resolution of the lines: $\Delta E/\sigma$ (σ is the standard deviation of the measured line).[31] As can be seen from the study of Ref. 44, this quantity is responsible for the basic possibility of determining the amplitudes of Gaussian lines that are superimposed on each other if their positions in the spectrum (i.e., their energy) and their standard deviations are known. Then, irrespective of the mathematical procedure for decomposing the spectrum, the accuracy that can be

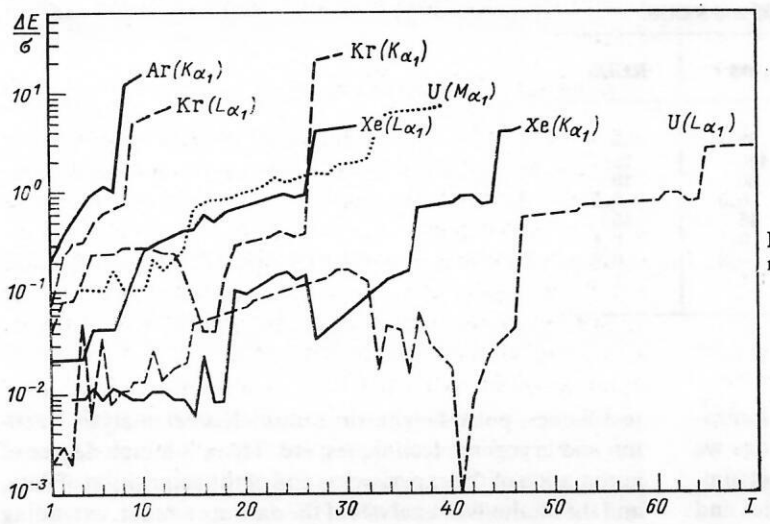

FIG. 25. Dependence of $\Delta E/\sigma$ on the degree of ionization I for x-ray K, L, and M transitions of some ions.

obtained for the amplitudes of the individual components is reduced by a factor

$$\varkappa \sim \left(\frac{1}{\Delta E/\sigma}\right)^{K-1} \tag{36}$$

compared with the statistical accuracy of the measured spectrum (K is the number of lines that are superimposed).

Figure 25 shows curves for $\Delta E/\sigma$ as a function of the degree of ionization K for x-ray K, L, and M transitions of some ions. Since σ includes the natural widths ω_λ of the line, these curves give the limit for resolving neighboring (in I) satellite lines of ions with outer vacancies. The resolution of transitions when $\Delta E/\sigma < 1$ is significantly more difficult or impossible in the case of poor statistics in the measurement.

Additional broadening of the diffraction reflection of an x-ray line can be due to geometrical aberrations (see Sec. 4). They are often dominant under the real conditions of an experiment and determine the width of the measured lines.

The program VERDI[46] was used to calculate the geometrical widths Δ of the reflections for a focusing crystal-diffraction spectrometer in Johansson geometry. The crystals were assumed to be LiF(200) and $SiO_2(13\bar{4}0)$ and to measure 40×20 mm, the radius of the focal circle was $R_F = 324$ mm, and the entry slit of the spectrometer measured 0.1×10 mm.

If in (30) we take into account only $\omega_\lambda(\Delta\vartheta_\lambda)$ and the geometrical width $\Delta(\Delta\vartheta_A)$ and ignore the quality parameter $\Delta\vartheta_{cr}$ of the crystal, we can, using the same criterion as above, determine the geometrical limit for resolution of x-ray satellites for a definite crystal-diffraction spectrometer.[67] In Fig. 26, the hatched fields are the regions of ions I) in the ground states whose K_{α_1} and L_{α_1} lines can be resolved by the corresponding analyzing crystals. It can be seen that if only one crystal is used, only a restricted range of ions can be covered, and this must be borne in mind when experiments are planned.

Such estimates of the possibility of resolving the lines of ions by means of a given crystal-diffraction spectrometer are important for understanding the natural or instrumental limits of measured quantities for characteristic transitions in ionized atoms and, therefore, for the consideration of the basic possibilities of the diffraction method for the purpose of diagnostics of ions sources.

We estimate the expected counting rate of events detected in a crystal-diffraction spectrometer corresponding to characteristic radiation of highly charged ions for the example of two focusing spectrometers whose parameters are given in Table V and which are denoted in this example by CDS and KCDS. For the ionization cross section, we choose $\sigma_K(Xe^{28+}) = 5\times10^{23}$ cm^2 and take K fluorescence yield $\omega_{101/2} \approx 0.9$ and weight of the K_{α_1} line $p_K \approx 0.6$. Using the expressions (14), (18), (31), (32), and (35), we obtain for the counting rate in the K_{α_1} line

$$\dot{N}_x = \frac{N_e^2 fc}{4\pi^3 a^2 R\bar{I}}\, T_R \sigma_K \omega_{nlj} p_K\, \frac{R_F}{b}\, \Gamma_\varepsilon T \sqrt{\omega_K^3 \sin 2\vartheta}\,, \tag{37}$$

where

$$\frac{R_F}{4\pi b}\, \Gamma\varepsilon T \sqrt{\omega_K^3 \sin 2\vartheta} = S \tag{38}$$

is the luminosity ot the spectrometers: $S(\mathrm{CDS}) \approx 3\times10^{-8}$ and $\mathrm{D(KCDS)} \approx 1.3\times10^{-8}$. It can be seen that the quality of the crystal plays an important part, since a more compact instrument can well have a poorer luminosity. With

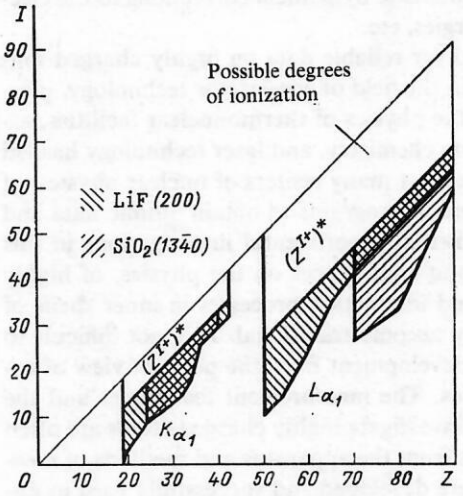

FIG. 26. Resolution limits for x-ray satellites (Ref. 67): $(Z^I)^*$ are excited ions, I is the degree of ionization, and Z is the atomic number.

TABLE V. Comparison of parameters of the spectrometers CDS and KCDS.

Parameter	CDS	KCDS
Radius R_F of focal circle, cm	32.4	15
Distance b from source to entry slit, cm	120	25
Mosaic effect of crystal, ω_{cr}, arc sec	30	10
Reflection coefficient Γ	0.5	0.5
Angle of observation ϑ, deg	45	45
Geometrical factor T_R (13) of the ring	0.1	0.1
Counter efficiency ϵ of CDS	0.8	0.8
Transmission T of radiation	1	1

allowance for the time of observation of the degree of ionization and the frequency 1 Hz of formation of the rings we obtain in the line about 1 event in 1 sec. To use the spectrum-analyzing programs, one needs both sufficient statistics and a sufficient width of the lines (several channels). In addition, it is necessary to have a definite number of measurement points near peaks in order to count the background events.

It follows from these estimates that physics experiments using the electron–ion rings of a collective heavy-ion accelerator and the crystal-diffraction method present a complicated problem, the successful resolution of which requires a further increase in the source intensity, optimization of all the parameters of the crystal-diffraction spectrometer, and a stable regime of measurement. It is essential to have a high degree of automation of the experiment to control and regularly monitor the spectrometer and to collect, store, and analyze the measured data.

6. SOME TOPICAL APPLICATIONS OF INVESTIGATIONS WITH ELECTRON–ION RINGS

During the last decade, the atomic physics of highly charged heavy ions has become an independent, rapidly developing field of theoretical and experimental investigations. The development of ion sources based on the use of accelerators has made it possible to perform new experiments to test the existing model ideas about the electron structure of the shells in ionized atoms, about the fundamental interactions in the strong electric field of the nucleus, about the part played by the relativistic dynamical corrections to the electron binding energies, etc.

The demand for reliable data on highly charged ions from specialists in the field of accelerator technology, plasma physics and the physics of thermonuclear facilities, astrophysics, plasma chemistry, and laser technology has led to the development, at many centers of nuclear physics, of independent research programs to obtain atomic data and carry out fundamental experimental investigations in this field. Symposia and conferences on the physics, of highly charged atoms and interaction processes in inner shells of ions have already become traditional. It is not difficult to understand this development from the point of view of experimental physics. The measurement techniques and the methods used to investigate highly charged atoms are often not very different from the apparatus and methods of measurement that were developed and successfully used in nuclear-physics investigations. One characteristically uses crystal and gas detectors, magnetic spectrometers, timing techniques, pulse-height–time multichannel analysis, vacuum and cryogenic techniques, etc. There is a high degree of automation of the experiments and of the acquisition of data, and the methods of analysis of the data are similar, extending to the creation of libraries of theoretical, experimental, or estimated data. It can be asserted that the investigations of highly charged ions on an extensive scale have only just commenced, and it is difficult to overestimate the prospects in this field of physics.

We shall dwell on only some of the proposals for physics experiments that appear to us at the present stage to be the most topical and realistic for performing with electron–ion rings and which are realized by the use of high-resolution x-ray spectrometers.

Energies of radiative transitions and their shifts

At the present time, there is a large amount of computational data for ionized atoms, in particular the energies of characteristic lines and their shifts as a function of the degree of ionization. Since the lifetime of inner vacancies ($\sim 10^{-16} - 10^{18}$ sec) is appreciably shorter than the time between two ionization events in electron–ion rings, the energy shifts of lines for the ground states of ions (satellites with outer vacancies) were calculated in Ref. 36. Relativistic calculations of the energy shifts have a high degree of accuracy because the necessary corrections to the electron binding energies give in this case an error of only second order.

At the same time, systematic verifications used for the calculations of the models[1] do not yet exist. Whereas, for example, the energies of x-ray K transitions in light ions are well described by even the nonrelativistic theory, it is to be expected that with increasing Z the relativistic effects will increase strongly and that it will no longer be possible to regard them as small corrections in the sense of perturbation theory.

In relativistic calculations, an important part is played by the dynamical two-particle corrections corresponding to the Breit interaction. It takes into account magnetic effects and retardation effects. The radiative quantum-electrodynamical corrections in accordance with the simplest diagrams of the interaction of the electrons with the self-field (self-energy) and with the field of the nucleus (vacuum polarization) have, in accordance with the dependence $\sim 1/n^3$ on the principal quantum number, a significant influence only on the lowest levels of the ions, i.e., on the energies of transitions in the K series. In addition, for heavier ions with $Z \geqslant 70$–80 it is necessary to take into account the finite size of the nucleus.

These effects make a contribution to the total energy of

an ion of order 1–10 eV, i.e., they correspond to quantities that can be measured by the proposed method. It is interesting to make systematic investigations for a wide range of Z and I. For example, the single-particle corrections to the energy in perturbation theory increase as $\sim Z^4$, and the two-particle corrections as $\sim Z^3$ for hydrogenlike ions,[68] and the quantum-electrodynamical corrections of lowest order are proportional to Z^4.

If it is assumed approximately that the x-ray transitions of the K series can be resolved by means of a crystal-diffraction spectrometer beginning with a degree of ionization $I \geqslant Z/2$, then in an experiment it is above all necessary to use a high-intensity source.

Ionization cross sections of ions

The calculations of the time development of the degree of ionization in an electron–ion ring made in Ref. 27 with allowance for the cross sections of single and double ionization were based on the kinetic equations

$$\frac{dN_I}{dt} = \sum_{J=0}^{I-1} K_{IJ}N_J - K_{II+1}N_J \quad I = 1, 2, \ldots, Z-1; \quad (39)$$

$$\frac{dN_Z}{dt} = \sum_{J=0}^{Z} K_{ZJ}N_J,$$

where the probabilities of transition from the lower state J to the state with charge I are given by the coefficients

$$K_{IJ} = \frac{1}{V} N_e v_e \sigma(Z_I, Z_J) \quad (40)$$

[V is the volume of the ring, v_e is the electron velocity, $\approx c$, and $\sigma(Z_I, Z_J)$ is the cross section for transition from Z_I to Z_J], and the probability of transition to the following charge state, $Z_I \to Z_{I+1}$ is

$$K_{II+1} = \frac{1}{V} N_e v_e \sigma(Z_I). \quad (41)$$

Here, as initial conditions the number of neutral atoms in the ring has been taken to be

$$N_0\ (t = 0) = \text{const} \quad (42)$$

and

$$N_I\ (t = 0) = 0,\ I = 1, 2 \ldots$$

Since in the volume of the compression chamber there is a finite pressure of the residual gas, it is in fact also necessary to take into account the flux of the atoms of the neutral gas in the volume of the ring:[34]

$$\frac{dN_0}{dt} = \sqrt{\frac{3}{4\pi}} v A n_0 \quad (43)$$

(v is the thermal velocity of the atoms of the residual gas, n_0 is the density of the neutral atoms in the ring, and A is the surface of the ring). This leads to stringent requirements on the vacuum in the compression chamber ($\approx 10^{-10}$ mm Hg).[69]

The calculations are described in more detail in Ref. 24, in which allowance is also made for effects of charge exchange of the ions, which can have a strong influence on the yield of ions with high degrees of ionization. The calculations include the total ionization cross sections, which are taken from model calculations,[33] since measured data are not available. Measurement of the yields of characteristic x rays of the ions would make it possible to determine the number of ions of a given species in the ring in a definite time interval and to extract the corresponding values of the ionization cross sections by solving the inverse problem of ionization.[70]

Such measurements were made earlier using the electron-beam ionizer KRION[4] for light ions. An advantage of an electron–ion ring is that the higher energy of the electrons makes ions of all Z and I accessible and makes it possible to study effects at large Z and I.

Diagnosis of electron–ion rings

Measurement of characteristic x rays of xenon ions in the electron–ion ring of a collective heavy-ion accelerator

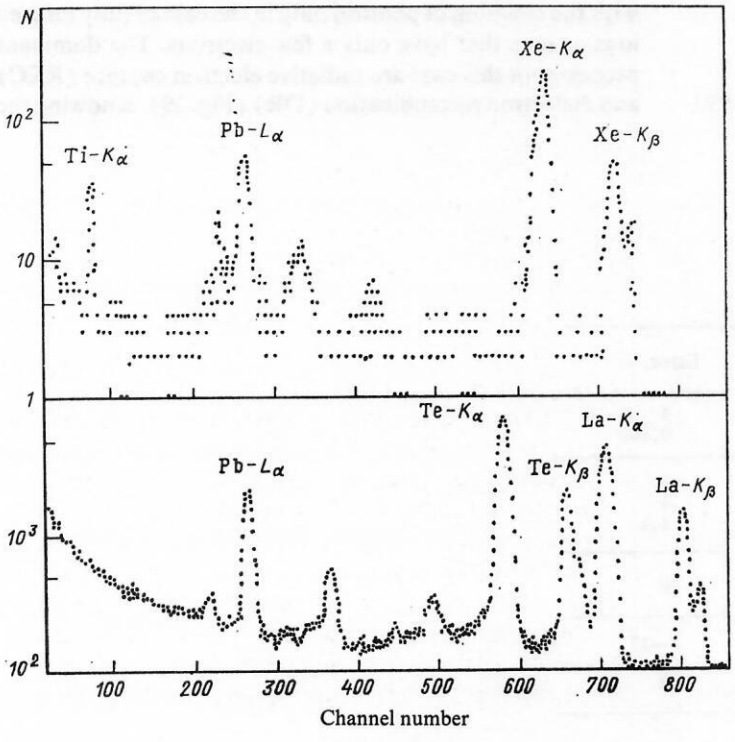

FIG. 27. Spectrum of characteristic x rays of the K line of xenon ions in an electron ring.[71] One can also see the Ti–K_α lines from the vacuum window of the accelerator and the Pb–L lines from the shielding lead. The lower part of the figure shows calibration lines of Te ($Z = 52$) and La ($Z = 57$).

(Fig. 27) was reported in Ref. 71. The conditions of the experiment did not permit detection of an energy shift of the lines, since the degree of ionization was low. The use of semiconductor detectors in this case did not permit resolution of the charge states of the ions. When the number of electrons in the ring is unknown, one can draw a conclusion from the number of detected x-ray events (37) about the product of the number of electrons and the number of ions in the ring:

$$\dot{N}_x \sim \frac{N_e^2 f}{\bar{I}} = N_e N_I. \tag{44}$$

When the number of electrons is known (for example, from measurements of the synchrotron radiation of the ring, $\Delta N_e/N_e \approx 20\%$), determination of the number of ions from $\dot{N}_x$ is possible for the initial stage of the ionization process, when the cross section for ionization of the K shell of low-charge ions, σ_K, hardly changes with the degree of ionization,[28] and the shifts of the lines are less than the resolution of the spectrometer.

The crystal-diffraction method makes it possible to obtain information about the distributions of the individual charge states of the ions, particularly highly charged ions, and about the variation of these distributions during the lifetime of the ring. For this, it is necessary to combine a pulse-height analysis of the spectra of the characteristic x rays of the ions with a time analysis, i.e., with a measurement of the time of emission of the x ray, as is described in detail in Ref. 71. The number of detected x rays from ions of the measured degree of ionization, N_{xi}, during the time of observation can then be calculated from a system of equations like (39), and we obtain the mean ion charge in the ring in accordance with the formula

$$\bar{I} = \sum_{i=1}^{Z} N_i i / \sum_{i=1}^{Z} N_i. \tag{45}$$

It is here necessary to use realistic calculated data for the ionization cross sections σ_{Ki}, since the sum of the detected x-ray events in a definite line is made up of the individual charge components (37):

$$\dot{N}_x = \sum_{i=1}^{Z} \dot{N}_{x,i} = c_r \sum_{i=1}^{Z} S_i \sigma_{K_i} \omega_i P_{K_i} N_i N_e$$
$$\approx c_r \overline{S_{\omega_{cr}}} \bar{P}_{K_i} N_e \sum_{i=1}^{Z} \sigma_{K_i} N_i \tag{46}$$

(c_r is the geometrical coefficient of the ring). The single-channel method of measurement with a focusing crystal-diffraction spectrometer necessitates an increase in the time of measurement that corresponds to the number of lines.

Investigation of hydrogenlike and heliumlike ions

Interesting objects of study are hydrogenlike and heliumlike ions with large Z.[72] The Lamb shift of levels of the ions Kr^{35+} was observed in the study of Ref. 73 with a crystal-diffraction spectrometer with a flat crystal; the shift was revealed by an energy shift of the line K_α. The accuracy achieved in the experiment of about 1 eV made it possible to measure the difference between the energies of the lines down to the smallest values and to compare the experimental data with the results of calculations in accordance with Dirac's theory. This effect is associated with quantum-electrodynamical corrections to the energy levels, which because of the Z^4 dependence become measurable by the crystal-diffraction method for sufficiently large Z of the nucleus. Such measurements are a good test of the basic ideas of quantum electrodynamics. The experiments to measure the Lamb shift are reviewed in Table VI for the Lamb shift of ground states with $n = 1$ and for $(2^2S_{1/2})$–$(2^2P_{1/2,3/2})$ transitions.

X-ray spectrometry of heliunlike ions makes it possible to obtain information about the electron–electron interaction, in particular, about correlation effects.[74] It should be noted that the intensity of quadrupole transitions and transitions of other high multipolarities also increases with Z, so that they can be observed in excited hydrogenlike and heliumlike heavy ions. This situation is reflected in Fig. 28 for the hydrogenlike and heliumlike ions Z^{1e-} and Z^{2e-}, respectively.

Measurement of lifetimes and transition energies is a very common method in spectroscopy. However, for highly charged ions there exists a further possibility for determining the electron binding energies in ground and excited states—by analysis of the process of capture of free electrons. Free electrons are captured in processes associated with the emission of photons only in the case of fully ionized ions or ions that have only a few electrons. The dominant processes in this case are radiative electron capture (REC) and dielectron recombination (DR) (Fig. 29). Knowing the

TABLE VI. Errors in experiments to investigate the Lamb shift.

System	Lamb shift	Z range	Error, %
Z^{1e-}	$n=2$	15—18 16	1 0,25
	$n=1$	16—36 36 18	15 4 1,4
Z^{2e-}	$n=2$	92	10
	$n=1$	16—36 36 18	3—15 3 3

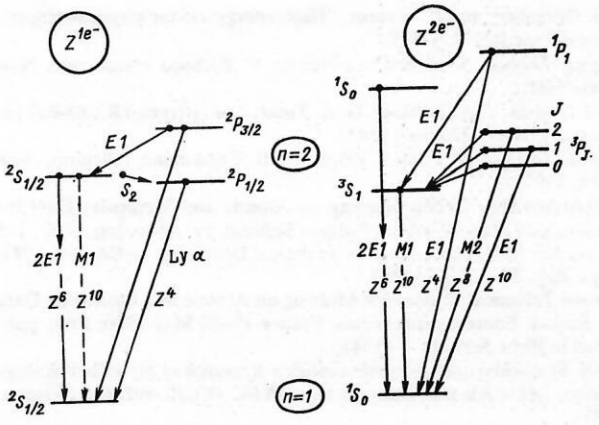

FIG. 28. Structure of hydrogenlike and heliumlike ions. The radiative transitions and their dependence on the atomic number Z are shown.[75]

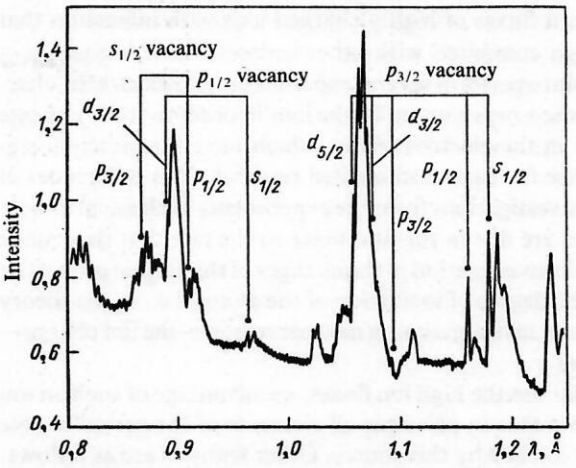

FIG. 30. The L spectrum of x rays from the heliumlike ions Bi^{73+} (Ref. 77).

conditions of electron capture, one can determine the total binding energies in ground states (by REC) and in doubly excited states (by DR).

Neonlike systems and other isoelectron series

The properties of the various isoelectron series of heavy ions having more electrons than heliumlike ions are of fundamental interest for investigations relating to the development of thermonuclear facilities.[14,15] Increasing interest is also shown in neonlike systems in connection with the development of short-wave lasers.[76] As an example of an experiment, Fig. 30 shows the L spectrum of the characteristic x rays of neonlike Bi^{73+} (Ref. 77). A feature of neonlike systems is that the electrons are in much stronger effective fields, so that the electron transitions occur with shorter wavelengths.

A clear enhancement of $L_{l+\alpha}$ radiation of Sm^{9+} relative to the L_{β_1} emission due to RTE processes was observed in Sm^{9+}–Xe collisions in Ref. 78 (Fig. 31). Such enhancement processes may open up a way to create presently unknown sources of coherent radiation. Therefore, the possibilitiies of the proposed investigations for other collisions and different elements are of great interest.

Investigations of dynamical processes in ion–atom or ion–ion interactions

Together with the extraction of electrons from the chamber of the compression chamber and additional acceleration there are some possibilities for performing experiments in order to investigate the dynamical processes in the electron shells of ions of different degrees of ionization: investigation of processes of multiple ionization by ion impact; differential investigation of processes of multiple ionization by ion impact; investigation of the dependence of the ionization of subshells on the impact parameter; investigation of coherent excitation in collisions with atoms of a noble gas; measurement of the lifetime of unstable ions; measurement of the probability of decay of K^{-2} vacancies; determination of fluorescence yields in L subshells; investigation of charge-exchange processes (differential cross sections, correlated capture of two electrons); investigation of resonance capture and excitation; investigation of neutralization radiation of hydrogenlike and heliumlike ions as a result of interaction with solid targets.

7. CONCLUSIONS

The use of electron–ion rings as a unique source of highly charged heavy ions opens up the possibility of obtaining

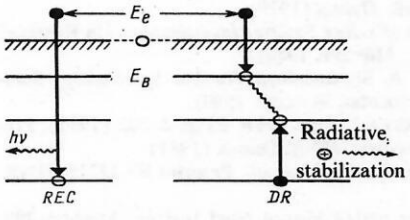

FIG. 29. Schemes of radiative electron capture (REC) and dielectron recombination (DR) (E_e is the electron energy, and E_β is the energy of the level).

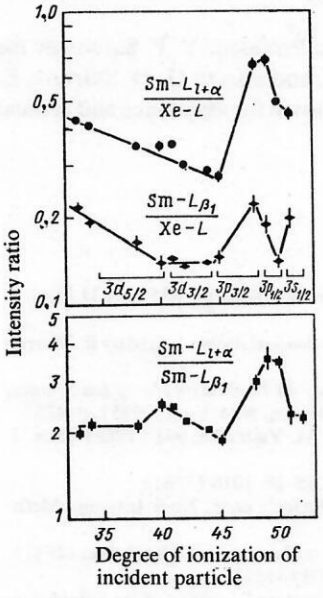

FIG. 31. Ratio of intensities of the x rays resulting from Sm^{9+}–Xe collisions at 3.6 MeV/nucleon.[78]

sufficient fluxes of highly charged ions with intensities that are high compared with other sources. On this basis, it is possible to perform several experiments to measure the characteristic x rays emitted by the ions in order to study delicate effects in the electron shells, which have fundamental significance for basic and applied research. The differences of these investigations from the experiments of classical atomic physics are due in the first place to the fact that they make possible investigation of the changes of the atomic properties with the degree of ionization of the atoms, i.e., in the theory of atomic investigations a new parameter—the ion charge—appears.

Besides the high ion fluxes, an advantage of such an ion source is that in principle all elements of the periodic table can be ionized by this source. Other features are as follows:

The ion charge dispersion varies with the time of accumulation of the ions in the ring, so that if special time regimes of measurement are used, it is possible to make measurements for different charge dispersions of the ions of a given element.

Measurements can be made during the time of developing ionization or after slow extraction of the ring from the compressor chamber, i.e., one can make measurements within the electron ring or measurements of interaction of the ion component with external targets after separation of the electron component of the ring.

Because the time between two ionization or excitation events is longer by several orders of magnitude than the characteristic time of de-excitation of all ions, the characteristic x rays which are observed are emitted by ions in their ground states. This fact greatly simplifies the interpretation of the measured x-ray spectra.

The energy of the electrons is so high that electrons can be knocked out of the deepest levels of the heaviest ions. However, the high energy of the electrons is simultaneously a shortcoming, since the ionization cross sections in such an energy range are far from the desired value.

We have demonstrated a number of advantages of x-ray spectrometry based on electron–ion rings; it obviously opens up a possibility for making experiments in the most topical fields of atomic physics.

We are deeply grateful to Professor V. P. Sarantsev for constant support in the work, and also to G. D. Shirkov, É. A. Perel'shteĭn, and V. M. Golovin for assistance and critical comments.

[1]G. Zschornack, Fiz. Elem. Chastits At. Yadra **14**, 835 (1983) [Sov. J. Part. Nucl. **14**, 349 (1983)].
[2]H. Winter, *Atomic Physics of Highly Ionized Atoms*, edited by R. Marrus (Plenum, New York, 1982).
[3]Martinson, "Beam foil spectroscopy," in *Treatise on Heavy Ion Science, Vol. 5*, edited by D. A. Bromley (Plenum, New York, 1985), p. 425.
[4]E. D. Donets, Fiz. Elem. Chastits At. Yadra **13**, 941 (1982) [Sov. J. Part. Nucl. **13**, 387 (1982)].
[5]J. Arianer, IEEE Trans. Nucl. Sci. **NS-28**, 1018 (1981).
[6]J. Ullrich, H. Schmidt-Bocking, S. Kelbch, *et al.*, Nucl. Instrum. Methods B **23**, 131 (1987).
[7]V. B. Kutner, Preprint R9-81-139 [in Russian], JINR, Dubna (1981).
[8]K. S. Golovanskiĭ, At. Energ. **56**, 303 (1984).
[9]R. Keller, "Heavy ion source development," in *Proc. of the Symposium 10 Years of Uranium Beam at the UNILAC*, edited by N. Angest and P. Klienle, GSI, 2–4 April, 1986, GSI-86-9 (Darmstadt, 1986).
[10]J. S. Greenberg and F. Vincent, "High-energy atomic physics—experimental," see Ref. 3, p. 141.
[11]*Atomic Physics: Accelerators*, edited by P. Richard (Academic, New York, 1980).
[12]E. D. Donets, V. A. Trifonov, G. A. Tutin, *et al.*, Preprint R7-83-627 [in Russian], JINR, Dubna (1983).
[13]*Atomic Inner-Shell Physics*, edited by B. Crasemann (Plenum, New York, 1985).
[14]IAEA Advisory Group Meeting on Atomic and Molecular Data for Fusion, held at the UKAEA Culham Laboratory, Abingdon, U.K., 1–5 November 1976; Proc. issued as Technical Document IAEA-199, 1977; Phys. Rep. **37**, No. 2 (1978).
[15]Second Technical Committee Meeting on Atomic and Molecular Data for Fusion, Fontenay-aux-Roses, France 19–22 May 1980; Proc. published in Phys. Scr. No. 2 (1981).
[16]N. N. Semashko *et al.*, *Atomic Collision Research in the eVkeV Energy Region, IAEA Nuclear Data Section, INDC (CCP)-192/GA* (Vienna, 1983).
[17]K. Katsonis, *Atomic Collision Data for Diagnostics of Magnetic Fusion Plasmas, IAEA Nuclear Data Section INDC(NDS)-160/GA* (Vienna, 1984).
[18]J. G. Hughes, *Atomic Data for Fusion Plasma Modeling, IAEA Nuclear Data Section, INDL(NDS)-177/GA* (Vienna, 1986).
[19]E. Hinnov, "Spectroscopy of highly ionized atoms in the interior of Tokomak plasma," in *Atomic and Molecular Processes in Controlled Thermonuclear Fusion*, edited by M. R. C. McDowell and A. M. Ferendeci (Plenum, New York, 1980), p. 449.
[20]E. Hinnov, "Highly ionized atoms in Tokomak discharges," in *Atomic Physics of Highly Ionized Atoms*, edited by R. Marrus (Plenum, New York, 1983), p. 49.
[21]B. Denne, *The Role of Atomic Spectroscopy in Fusion Research, Abstracts of the 20th EGAS* (Graz, 1988), p. 168.
[22]R. L. Blake and L. L. Houser, Astrophys. J. **149**, L133 (1967).
[23]V. P. Sarantsev and E. A. Perel'shteĭn, *Collective Acceleration of Ions* [in Russian] (Atomizdat, Moscow, 1979).
[24]É. A. Perel'shteĭn and G. D. Shirkov, Fiz. Elem. Chastits At. Yadra **18**, 154 (1987) [Sov. J. Part. Nucl. **18**, 64 (1987)].
[25]G. Musiol and G. Zschornack, Wiss. Z. Tech. Univ., Dresden **37**, 99 (1988).
[26]G. Zschornack and G. Musiol, Kernenergie **31**, 291 (1988).
[27]D. Lehmann, G. Muller, G. Musiol, *et al.*, Preprint 9-10744 [in Russian], JINR, Dubna (1977).
[28]G. Zschornack and G. Musiol, Preprint R13-12540 [in Russian], JINR, Dubna (1979).
[29]G. Zschornack, N. I. Zamyatin, D. Lehmann, *et al.*, Preprint R13-12541 [in Russian], JINR, Dubna (1979).
[30]G. Zschornack, G. Musiol, and G. Müller, Preprint R13-12542 [in Russian], JINR, Dubna (1979).
[31]G. Zschornack, "Entwicklung der Theorie und Messmethodik in den Elektron-Ionen-Ringen des Schwerionenkollektivbeschleunigers des VIK Dubna auftretenden charakteristischen Roentgenstrahlung für die Untersuchung der Huellenstruktur hochionisierter Atome," Dissertation B, Techn. Univ., Dresden (1984).
[32]W. Wagner V. B. Dunin, G. Karrasch, *et al.*, Kratk. Soobshch. No. 6-85 [in Russian], JINR, Dubna (1985).
[33]H. W. Siebert, D. Lehmann, G. Musiol, *et al.*, Preprint R9-10197 [in Russian], JINR, Dubna (1976).
[34]É. A. Perel'shteĭn and G. D. Shirkov, Preprint E9-85-4, JINR, Dubna (1985).
[35]É. A. Perel'shteĭn and G. D. Shirkov, Preprint E9-88-238, JINR, Dubna (1988).
[36]G. Zschornack G. Musiol and W. Wagner, Report ZFK-574, Rossendorf (1986).
[37]G. Zschornack, G. Musiol, and R. Pitz, Preprint R7-83-57 [in Russian], JINR, Dubna (1983).
[38]G. Zschornack, Phys. Scr. **3**, 194 (1983).
[39]G. Zschornack, Nucl. Instrum. Methods B **23**, 278 (1987).
[40]N. B. Kazarinov, V. I. Kazacha, and E. A. Perel'shteĭn, Preprint R9-12719 [in Russian], JINR, Dubna (1979).
[41]M. A. Blokhin, *Methods of x-Ray Spectral Investigations* [in Russian] (Gosizdat Fiz.-Mat. Lit., Moscow, 1959).
[42]B. S. Dzhelepov and S. A. Shestopalova, *Nuclear Spectroscopy Standards* [in Russian] (Atomizdat, Moscow, 1980).
[43]A. Pohlers and G. Zschornack, Prib. Tekh. Eksp. **2**, 202 (1983); Preprint R13-81-794 [in Russian], JINR, Dubna (1981).
[44]G. Müller, D. Lehmann, G. Musiol, *et al.*, Preprint E7-12219, JINR, Dubna (1979).
[45]G. Zschornack, G. Müller, and G. Musiol, Nucl. Instrum. Methods **200**, 481 (1982).
[46]A. Reichmann, G. Musiol, W. Wagner, *et al.*, Preprint TU 05-01-87 Technische Universität, Dresden (1987).

[47]G. Karrasch, G. Zschornack, R. Bandisch, *et al.*, Preprint R13-83-473 [in Russian], JINR, Dubna (1983).
[48]G. Karrasch, G. Zschornack, V. B. Dunin, *et al.*, Preprint R13-83-474 [in Russian], JINR, Dubna (1983).
[49]G. Musiol, G. Zschornack, and W. Wagner, Gemeinsamer Jahresbericht, 1982, ZFK-503, Rossendorf (1982).
[50]G. Karrasch, R. Kirchbach, W. Schulze, *et al.*, Preprint R13-83-484 [in Russian], JINR, Dubna (1983).
[51]G. Müller, R. Pitz, and G. Zschornack, Preprint R13-81-698 [in Russian], JINR, Dubna (1981).
[52]G. Müller, G. Karrasch, and G. Zschornack, Preprint R13-83-55 [in Russian], JINR, Dubna (1983).
[53]Inkrementales Durchlichtlaengenmessystem IDL 1. Firmenschrift VEB Carl Zeiss Jena, Jena (1982).
[54]Inkrementales Durchlichtwinkelmessystem IDW, Firmenschrift VEB Carl Zeiss Jena, Jena (1982).
[55]U. Todt, Praktikumsarbeit, Technische Universität Dresden, Sektion Physik, Wissenschaftsbereich Angewandte Kernphysik, Dresden (1984).
[56]A. Reichmann, Diplomarbeit, Technische Universität Dresden, Sektion Physik, Dresden (1984).
[57]W. Schwitz, J. Kern, and R. Lanners, Nucl. Instrum. Methods **154**, 105 (1978).
[58]K. V. Anizovich, Prib. Tekh. Eksp. No. 1, 228 (1981).
[59]J. J. Reidy, "Curved Crystal Spectrometers," in *The Electromagnetic Interaction in Nuclear Spectroscopy* (North-Holland, Amsterdam, 1975), p. 839.
[60]Y. Cauchois and C. Bonelle, "X-ray Diffraction Spectrometry," in *Atomic Inner Shell Processes, Vol. II* (Academic Press, New York, 1975), p. 83.
[61]M. O. Krause and J. H. Oliver, J. Phys. Chem. Ref. Data **8**, 329 (1979).
[62]M. A. Blokhin and I. M. Shueĭtser, *Handbook of x-Ray Spectroscopy* [in Russian] (Nauka, Moscow, 1982).
[63]G. Zschornack, A. Pohlers, and A. Reichmann, Preprint R10-83-75 [in Russian], JINR, Dubna (1983).
[64]W. Beer, IPF-SP-004, Fribourg (1974).
[65]G. Zschornack, Atomdaten für die Roentgenspektralanalyse, VEB Deutscher Verlag für Grundstoffindustrie, Leipzig (1989).
[66]A. Reichmann, G. Zschornack, and W. Wagner, Wahrscheilichkeitstheoretische Beschreibung von Geometrieeinfluessen auf die Parameter von Bragg-Kristalldiffraktionsspektrometern, EAS-6-Kassel (1985), p. 191.
[67]W. Wagner and G. Zschornack, "Separation of outer shell satellite x-ray lines of sources of highly ionized atoms," Annual Report 1985, ZFK-384, Rossendorf (1985), p. 117.
[68]I. P. Grant, Comput. Phys. Commun. **17**, 149 (1979).
[69]É. A. Perel'shteĭn and G. D. Shirkov, *Symposium on Problems of the Collective Method of Acceleration*, D9-82-664 [in Russian] (JINR, Dubna, 1982), p. 31.
[70]B. Bochev, V. P. Ovsyannikov, and T. Kutsarova, Communication R7-11567 [in Russian], JINR, Dubna (1978).
[71]G. Zschornack, G. Müller, and G. Musiol, Nucl. Instrum. Methods **173**, 457 (1980).
[72]M. W. Kugel and D. E. Murnick, Rep. Prog. Phys. **173**, 457 (1977).
[73]J. P. Briand, P. Indelicaba, M. Tavernier, *et al.*, Z. Phys. A **318**, 1 (1984).
[74]R. D. Cowan, *The Theory of Atomic Structure and Spectra* (University of California, Berkeley, 1981).
[75]P. H. Mokler, *Information on the Structure of Heavy Few-Electron Ions, GSI, Darmstadt* (Darmstadt, 1987).
[76]R. Bock, G. Kessler, and S. Witkowski, "High energy in matter produced by heavy ion beams," Annual Report, GSI, Darmstadt (1986), p. 87.
[77]D. D. Dietrich, G. A. Chandler, R. J. Fortner, *et al.*, Nucl. Instrum. Methods **B9**, 686 (1985).
[78]W. A. Schoenfeldt, P. H. Mokler, and D. H. H. Hoffman, Z. Phys. D **4**, 161 (1986).
[79]A. Salop, Phys. Rev. A **8**, 3032 (1973).
[80]A. Salop, Phys. Rev. A **9**, 2496 (1974).
[81]G. D. Shirkov, Preprint R9-12055 [in Russian], JINR, Dubna (1978).
[82]É. A. Perel'shteĭn and G. D. Shirkov, Preprint R9-82-526 [in Russian], JINR, Dubna (1982).

Translated by Julian B. Barbour